Geophysics Open-File Report 10
Geoscience Department
New Mexico Tech
Socorro, NM 87801

THE USE OF MICROEARTHQUAKES TO MAP AN EXTENSIVE MAGMA BODY IN THE SOCORRO, NEW MEXICO AREA

by

Eric J. Rinehart

Submitted in partial
fulfillment
of
the requirement
of
Geophysics 590
and the
Master's Degree Program
at
New Mexico Institute
of
Mining and Technology

December 1976

The research described in this paper was sponsored jointly by the National Science Foundation (DES74-24187) and the State of New Mexico (Board of Educational Finance (BEF-6) and Energy Resource Board (ERB-75-300)).

ABSTRACT

The primary purpose of this study was to determine the lateral extent and relief of the upper surface of an extensive magma body detected by Sanford and Long (1965) and Sanford and others (1973). A five to six station, movable array of seismographs was employed throughout the Socorro, New Mexico, area from April, 1975, to September, 1976. High gain (approximately 10^6 magnification at 40 H_Z), vertical component seismographs were used to find 163 hypocenters which represented locations for 645 shocks because 70 percent of all the shocks occurred in earthquake swarms.

Hypocenters were diffusely distributed within the Rio Grande Rift with no apparent clustering along faults. The geographic distribution of epicenters, particularly those for earthquake swarms, correlated well with the lateral extent of a magma body located approximately 18 km below the surface.

The shear waves produced by the microearthquakes provided S_ZS reflections from the extensive magma layer. Using the reflection times and locations, good resolution of the extent and relief of the magma body was obtained below 34.12°N. The southern boundary, which extends southward to approximately 34.00°N, is highly irregular.

The minimum depth to the body is approximately 18 km beneath Socorro Mountain and deepens to approximately 20 km below the surface at the magma body's margins. The data

suggest a north-south orientation for the magma body with the axis following beneath the Socorro-Lemitar Mountain block.

INTRODUCTION

For some time (see Sanford and Long, 1965, and Sanford and others, 1973), the existence and a minimum extent of an extensive magma body approximately 18 km beneath Socorro, New Mexico, have been known. The exact dimensions of this body, however, have never before been established.

The primary purpose of the study reported in this paper was to determine the configuration of the magma body using S_ZS reflections from the top of the magma layer as recorded on microearthquake seismograms. Another goal of the research was to determine the relation between the distribution of microearthquake hypocenters and magma bodies--the small shallow ones proposed by Shuleski (1976) as well as the deeper extensive magma body.

Microearthquake data for this study were obtained with a movable array of 5 to 6 seismograph stations during the period April, 1975, to September, 1976. Because accurate hypocenters were essential in determining the relief on the upper surface of the magma body, considerable effort was made to estimate errors in location, and to categorize events according to the estimated errors. Data from the best located events were used then to map the magma layer.

PREVIOUS GEOLOGICAL AND GEOPHYSICAL STUDIES

Socorro, New Mexico, is located in the Rio Grande Rift, a large, extensional structural feature running from southern New Mexico to central Colorado. The rift, consisting of a series of linked structural depressions with raised margins, is locally cut through by an intergraben horst extending from 50 km north to 30 km south of Socorro. These horsts, existing for only a small fraction of the total rift length, are thought to be only 12-10 million years old and, by themselves, may suggest a recent anomaly in the crustal structure at Socorro (Chapin and Seager, 1975). Figure 1 shows general surface features in the Socorro area. For more information about the geology of the Rio Grande Rift, Chapin and Seager (1975) and Mott (1976) should be consulted.

The first geophysical evidence of any crustal anomaly was presented by Sanford and Long (1965) who found that many local microearthquake seismograms contained 2 sharp arrivals at an average of 2.5 and 5.0 seconds, respectively, after the direct S wave arrival. Time-distance graphs for the two arrivals were constructed and the arrivals were identified as (1) S_ZP (an S to P wave reflection) and (2) S_ZS (an S to S wave reflection), both being reflected from a discontinuity approximately 18 km below the surface. No incident P waves were found to be reflected from the discontinuity; however, if they did exist, they may have been masked by other seismic signals.

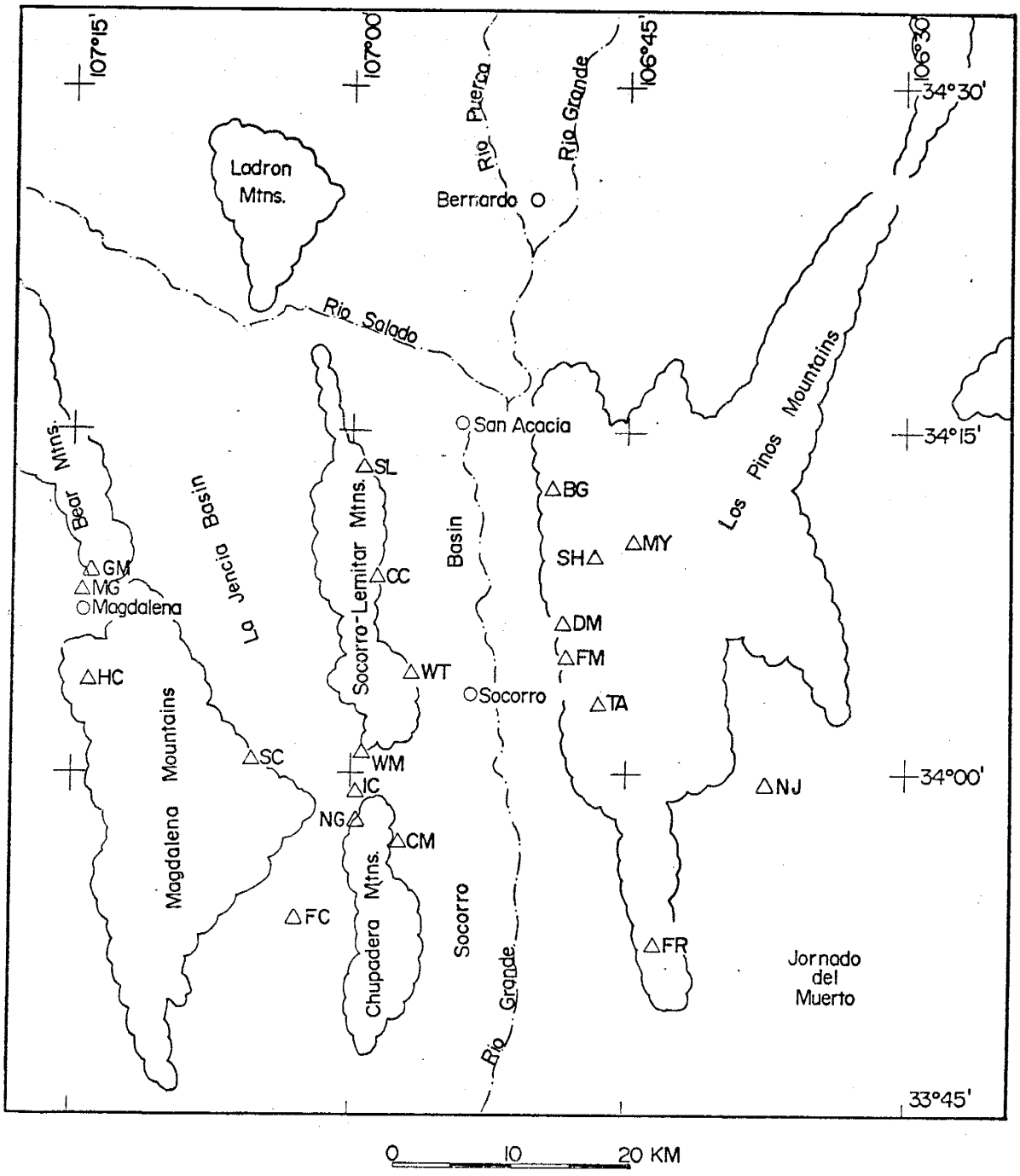

Figure 1. Map of the Socorro, New Mexico, area showing station locations and outlines of physiographic features (From Sanford, and others, 1976).

Sanford and others (1973) substantiated the existance of the discontinuity. Employing alternate means, they established its depth below Socorro to be 17.8 km and, including seismograms from a station near Albuquerque (ALQ), extended the discontinuity approximately 60 km north of Socorro. They found that the observed S_ZP to S_ZS ratios could only be explained by a change in phase of the rock--from solid to molten--at the 18 km discontinuity. This suggested that the discontinuity was the top boundary of an extensive magma body. The high frequency content of the reflections indicated that the boundary was quite sharp.

Beginning in early 1975, a program was started at NMIMT to identify any small, shallow (minimum depths $<$10 km) magma bodies that might be fed by the extensive chamber at 18 km below the surface. Shuleski (1976) found that the SV waves for some microearthquakes in the Socorro region were very small at some recording stations and fault mechanisms of the microearthquakes could only explain about 40 percent of these observations. To explain the remaining 60 percent, five small, shallow (depths less than about 7 km) magma bodies were proposed (see Figure 2) to reduce the SV wave amplitudes through S wave screening.

By reducing data from primary level lines that ran from El Paso, Texas, to Albuquerque, New Mexico, Reilinger and Oliver (1976) found a high rate of surface uplift in the general area of the magma body proposed by Sanford and others (1973). The uplift, reaching a maximum average uplift rate

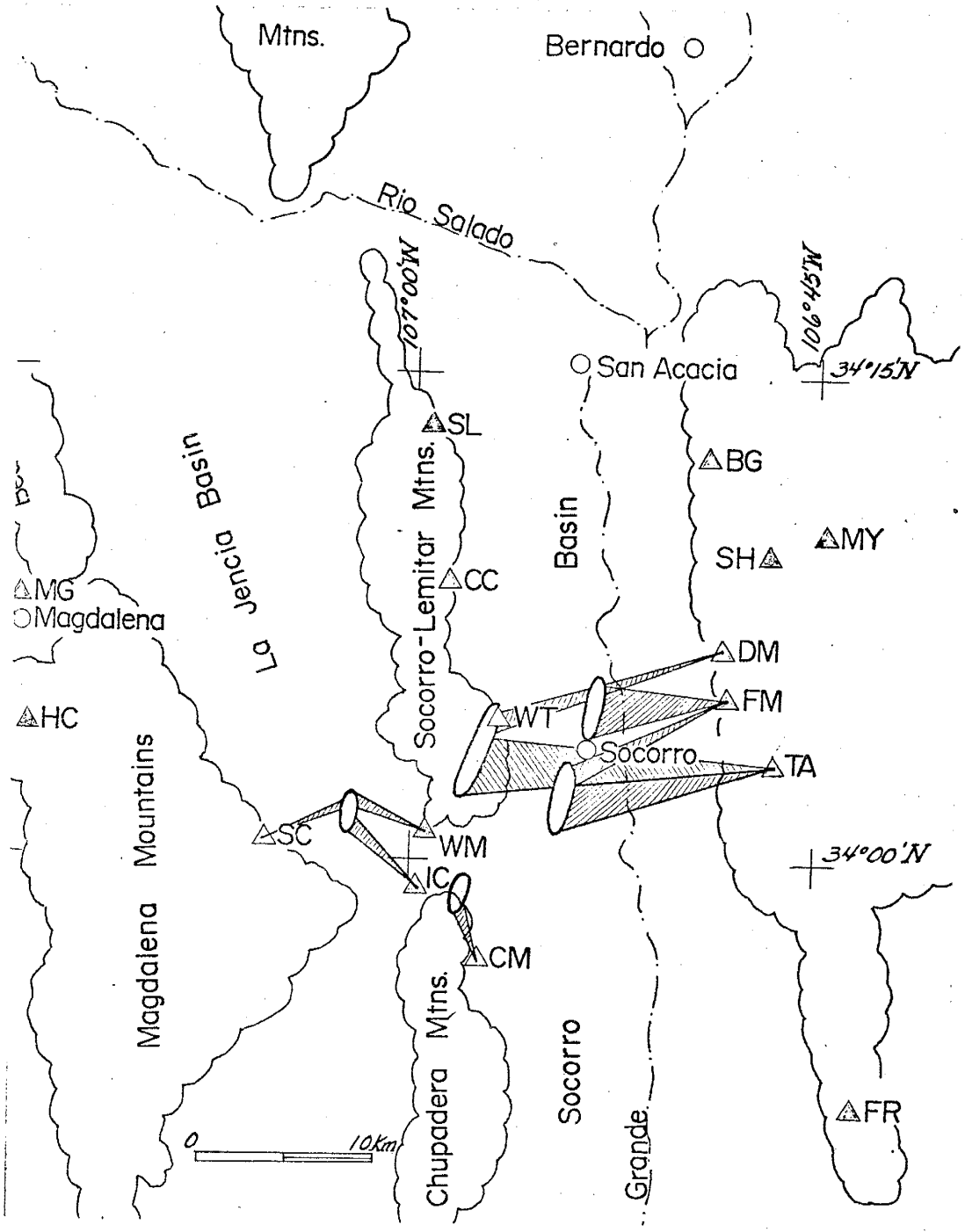

Figure 2. Location of five magma bodies that could explain observed SV wave screening (After Shuleski, 1976)

of 6.1 mm/yr 23 km north of Socorro and decreasing to about 3.2 mm/yr about 55 km north of Socorro, extends from 20 km south to 50 km north of Socorro.

INSTRUMENTATION

Two basic systems were used throughout this study. For the location of hypocenters and studies of magma bodies, an array of Sprengnether MEQ-800 seismic recording systems was used. For comparison of the reflected phase frequencies, the MEQ-800 records were used in conjunction with those from an LRSM system at station SNM. Descriptions of the MEQ-800 seismograph, the seismic array used and the LRSM system are given below.

Five to six portable MEQ-800 systems were available for use in a movable array which occupied the twenty-one different stations shown in Figure 1. The array, deployed on Mondays and retrieved on Fridays, relied upon station WT as its standard, while the remaining systems were arranged by the need to obtain data from particular areas.

The Sprengnether MEQ-800 recording system has a gain stable amplifier with gain settings ranging from 60-140 db in discrete 6 db intervals. Some filtering of the seismic signal is possible for both low frequencies (below 5 or 10 Hz) and high frequencies (above 5, 10, or 30 Hz). For this study, the 30 Hz setting on the high frequency filter was used over 50 percent of the time overall and 100 percent of the time for the noisiest stations (BG, CU, FC, FR, HC, SL, TA, MY). The filtering was necessary to reduce noise generated by wind and small rodents. The microearthquake signals were not

impaired by the filtering since the MEQ-800 system still had a very good response at this setting for frequencies around 30 Hz, the predominate frequency of the P arrival (Sanford and Holmes, 1962). Helical recording on smoked paper at a rate of 120±0.6 mm/min was used to record the seismic signatures.

Self-contained, quartz crystal chronometers were used for timing of seismic arrivals. These clocks were synchronized, at the beginning of each recording week, with the WWV standard time signal by simultaneously recording both signals. The clock drift, always less than 0.1 second per day, was considered to be linear and was determined for each unit on the last recording day, again by simultaneous recording with the WWV time signal. Recording rate variations and clock drift corrections were applied to all arrival times.

To complete the MEQ-800 system, either a Willmore vertical geophone (1.5 Hz natural frequency) or a Mark Products L4-C vertical geophone (1.0 Hz natural frequency) was used. Magnification response curves for both systems are shown in Figure 3 for the usual field settings. A peak magnification of around 2×10^6 is achieved at 40 Hz (with high filter set on 30). The response of the system was well suited for the high frequency, small amplitude signals produced by microearthquakes. The geophones were protected from extraneous noise and inclement weather by either being buried or being placed in a cave or mine.

The twenty-one stations occupied in this study (shown in Figure 1) are listed in Table 1 along with their locations

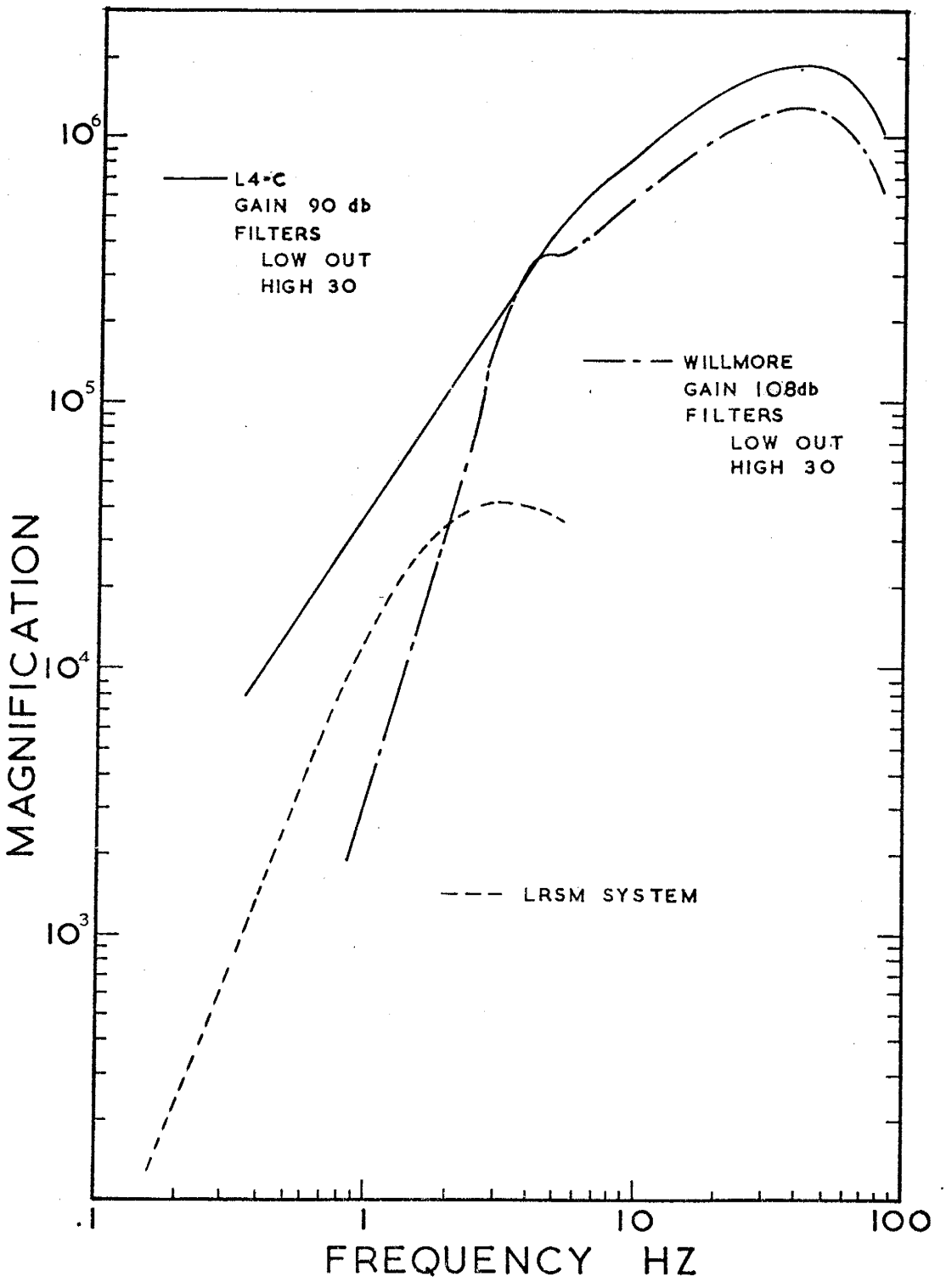

Figure 3. a. Response curves for the MEQ-800's with either a L4-C or Willmore geophone at field operating settings and b. response curve of the LRSM system at SNM.

TABLE 1. Portable Seismograph Station Locations.

Station	Latitude	Longitude	Elevation(m)
BG	34.2068	106.8205	1516
CC	34.1442	106.9812	1649
CM	33.9501	106.9576	1640
CU	34.1573	106.7785	1585
DM	34.1075	106.8079	1536
FC	33.8950	107.0504	1850
FM	34.0829	106.8047	1537
FR	33.8747	106.7270	1558
GM	34.1454	107.2345	1945
HC	34.0658	107.2361	2240
IC	33.9870	106.9967	1730
MG	34.1305	107.2425	2024
MY	34.1667	106.7459	1645
NG	33.9648	106.9933	1730
NJ	33.9924	106.6253	1644
RH	33.9002	107.1135	2080
SC	34.0100	107.0894	2073
SH	34.1570	106.7802	1577
SL	34.2234	106.9910	1615
TA	34.0498	106.7751	1558
WM	34.0120	106.9929	1673
WT	34.0722	106.9459	1555

and elevations. Protection from atmospheric noise was a main prerequisite for site selection. In most cases, caves and abandoned mines were utilized; however, six stations (HC, MY, CU, SL, TA, and NG) were only protected by rock overhangs. In all cases, underlying material of the stations was solid rock, reducing as much as possible seismic signals arriving nearly vertically by refraction through low velocity surface material.

The LRSM system, located at station SNM, consisted of 1 vertical and 2 horizontal (N-S and E-W) short period Benioff seismometers. The system employed Helical 35 mm film recording at a rate of 0.25 mm/sec. The response curve for normal operation is shown in Figure 3. The magnification had a peak value of about 40 k (included a 12x enlargement factor) at a frequency of 3.3 H_Z. The lower frequency response of the LRSM compared with the MEQ-800 allowed some qualitative frequency versus amplitude comparison of micro-earthquake signals.

DATA

1. Location Procedure

Before microearthquake data could be used to determine geophysical properties of the crust, good hypocenter locations were required. A primary effort of this research was to locate hypocenters accurately in space and time and to provide some estimate of possible errors contained in the resulting data.

The crustal model used throughout the study was a homogeneous half-space with a P wave velocity of 5.8 km/sec and a S wave velocity of 3.35 km/sec (or a Poisson's ratio of 0.25). Although a very simple model, it proved to be adequate primarily because distances between stations in the arrays occupied were small.

The data used for locations were the P and S wave arrival times. P wave arrival times, the most critical, were measured to an accuracy of ± 0.02 seconds with the use of a traveling microscope. S wave arrival times were measured with a millimeter scale providing an accuracy of ± 0.1 second. Usually all times were read twice.

When P and S wave arrival times were known for a particular event, an initial origin time was found from a Wadati diagram. In these diagrams, S-P times were plotted versus P arrival times. A line with a slope of 0.732 was fitted by eye through the data. The origin time was the abcissa intersect ($S - P = 0$) of the fitted line. If only four or three stations recorded the shock, the origin time found by the Wadati diagram was considered a known quantity and was fixed.

After an initial origin time was found, crude, initial spatial coordinates were determined using P wave travel times. These estimated coordinates, along with the actual P wave travel times, station locations, and crustal model were given to an iterative, inversion computer code from which a reliable hypocenter and a new origin time were obtained. Because four parameters were usually calculated, at least five arrival times were necessary to have the problem overdetermined. In these solutions, the iterative origin time was compared with the Wadati origin time. A difference of up to ±0.5 seconds was acceptable. If the difference was greater, the origin time was constrained to be within ±0.5 seconds of the Wadati origin time.

If only four arrival times were available, only the Wadati origin time was used. In this case, only three parameters remained unknown and the problem was still overdetermined.

After an iterative solution was obtained, it was compared with the hypocenter obtained from a computer adaptation of the graphical procedure described by Richter (1958, pp. 320-321). The only variable parameters in the graphical solution are the P wave arrival times. The fixed origin time used came from the iterative process. If the cluster of intersections was good and the location agreed well with the iterative solution, the exact iterative solution was accepted as the actual hypocenter and origin time. If the intersections of chords of the graphical solution were not satisfactory, the origin time was allowed to change, again within ±0.5 seconds of the

Wadati origin time. The origin time providing the tightest cluster of chord intersections was the adopted hypocenter. As the origin time must be specified, events with only four arrival times were best located with this technique. In addition, some three station locations were also found with this program but only for events which had excellent Wadati origin times.

2. Error Analysis

A quantitative analysis of location errors for five well-located microearthquakes was made. All five hypocenters were graded G or E (see next section). Four of the microearthquakes were chosen at random from events that had well-established hypocenters. These were used to determine possible errors arising from uncertainties in the crustal velocity and P wave arrival times. These four events had very small travel time residuals (observed less theoretical travel times); had nearly identical Wadati and iterative origin times; were contained within the recording array; and had one seismic station within 11 km of the epicenter. Locations of the four events are given in Tables 2 and 3. The fifth event was used in determing duplication of locations for the same earthquake. It was timed, located and checked as two different events before it was noted that both sets of times were actually for the same shock. Data for this shock are given in Table 4.

Table 2 lists derived hypocenters and iterative origin times for three shocks when the P wave velocity was altered by 0.1 km/sec increments from 6.2 km/sec to 5.4 km/sec.

TABLE 2. Change of Spatial Parameters and Origin Times Arising from a Change in the Velocity Model.

Date and Wadati Origin Time	Velocity	Origin Time	Latitude (°N)	Longitude (°W)	Depth of Focus (km)[1]	S.D.[2]
04-13-76[3]	6.0	11:41:26.03	34.0684	107.0515	1.9	0.25
11:41:25.7	5.9	25.81	.0449	.0538	5.6	.08
	5.8	25.93	.0477	.0522	4.5	<.05
	5.4	25.66	.0458	.0502	5.4	<.05
04-20-76[4]	6.1	08:32:19.16	34.0948	106.8387	2.4	0.10
08:32:19.2	6.0	19.17	.0957	.8407	2.8	.08
	5.8	19.11	.0976	.8424	3.0	.07
	5.7	19.08	.0992	.8422	3.0	.07
	5.6	19.05	.0994	.8429	3.0	.06
	5.4	18.98	.0999	.8443	3.1	.05
08-12-76[5]	6.2	04:56:05.46	34.0552	106.9900	6.9	<.05
04:56:05.2	6.0	05.33	.0603	.9863	7.7	<.05
	5.8	05.10	.0610	.9860	8.5	<.05
	5.6	04.86	.0615	.9861	9.7	<.05
	5.4	04.58	.0620	.9862	10.8	<.05

1 Depth below sea level.
2 Standard deviations of the travel time residuals (observed less theoretical times about a zero mean.
3 Closest station 7 km away
4 Closest station 3 km away
5 Closest station 11 km away

TABLE 3. Change of Spatial Parameters and Origin Times Arising from a + 0.1 Second Timing Error at Each Seismograph Station (V_p=5.8 km/sec).

Date and Wadati Origin Time	Station[1]	Origin Time	Latitude (°N)	Longitude (°N)	Depth of Focus (km)[2]	S.D.[3]
04-13-76	SC	11:41:25.77	34.0447	107.0481	6.2	<0.05
11:41:25.7	WM	25.65	.0464	.0545	6.7	.05
	IC	25.74	.0435	.0529	5.9	.05
	CC	25.86	.0421	.0512	5.2	.05
04-13-76	IC	11:58:34.54	33.9882	106.9486	6.2	<0.05
11:58:34.6	WM	34.60	.9884	.9500	5.3	.05
	CM	34.78	.9944	.9564	4.4	.05
	WT	34.65	.9878	.9548	5.3	.05
	CC	34.76	.9897	.9533	4.2	.05

1 Station whose P arrival time is changed by + 0.1 second.
2 Below sea level
3 Standard deviations of the travel time residuals (observed less theoretical times) about a zero mean.

Three basic conclusions were drawn:

(1) Depths of focus were the least accurately determined parameter.

(2) As the closest station's epicentral distance became larger, the depths of focus became more uncertain.

(3) In some instances, a 3 percent change in velocity could alter an event's classification. For example, the standard deviation of 0.25, observed for the for the shock on 04-13-76, would have required this event to be downgraded from a G to a B classification (see next section).

The effects of errors in arrival times at individual stations are shown in Table 3. P wave arrival times at successive stations, for two shocks were changed by +0.1 second. The effect on the origin times and spatial coordinates are listed in Table 3. Again, the least accurately determined parameter was depth of focus.

Data for the earthquake that was inadvertantly located twice are given in Table 4. Epicenter locations were within 15 seconds of arc, but the difference in the depth of focus was surprisingly large.

If a microearthquake had at least one close recording station (<6 km epicentral distance) then the depth of focus could be determined accurately from the closest station data. However, when all epicentral distances were greater than 20 km the depths of focus, especially for shallow events, became very difficult to establish. This difficulty increased as the epicentral distances became larger. An epicenter outside of

TABLE 4. Two Solutions for the Event Occurring on 01-23-76.

Iterative Origin Time	Latitude(°N)	Longitude(°W)	Depth of Focus(km)*
02:53:33.68	34.0296	107.0135	1.8
02:53:33.50	34.0282	107.0179	3.9

Wadati Origin Time: 02:53:33.2

* Below sea level

the array in conjunction with a large epicentral distance made the problem even more difficult.

CLASSIFICATION OF EVENTS

Because of the uncertainty of hypocenter locations, especially depths of focus, all events were evaluated and placed into three classes, E, G and B:

Class E--Excellent hypocenter locations (small travel time residuals). Events occur within the array; epicenters are less than 6.2 km from the nearest station; and depths of focus are determined only by the nearest station. Errors are $\pm\frac{1}{4}$km for epicenters and $\pm$1 km for the depths of focus. Class E microearthquakes are listed in Table 5.

Class G--Good hypocenter locations. Events occur within the array and have depths of focus determined by two methods, if possible. The errors are $\pm\frac{1}{2}$ km for the epicenter and $\pm$2 km for the depths of focus. Class G microearthquakes are listed in Table 6.

Class B--Uncertain hypocenter locations. Events have at least one of the following faults which makes its location uncertain: (1) epicenter is outside of the array, (2) residuals obtained in the iterative program are large, (3) insufficient data (e.g. only 3 stations). For this class of events, the epicenter errors do not exceed 5 km, but depths of focus are unobtainable. For computational purposes, Class B events are assigned depths of focus of either 3 km or 6 km, depending upon their location. Class B microearthquakes are listed in Table 7.

TABLE 5. Class E. Events.

Date	Origin Time	Latitude (°N)	Longitude (°N)	No. of Events	Depth* h_1	Depth* h_2
6-03-75	15:10:15.60	34.0301	107.0296	1	9.50	10.34
7-23-75	14:56:41.62	34.0281	107.0576	3	11.60	11.10
8-08-75	10:57:22.59	34.0796	106.9329	6	6.80	6.80
8-12-75	15:25:28.30	34.0513	106.9785	1	8.80	8.80
8-20-75	05:22:19.70	34.0882	106.9261	15	10.10	10.10
8-20-75	12:20:50.35	34.0833	106.9153	2	7.00	7.00
8-20-75	15:29:36.60	34.0848	106.9261	2	6.90	6.90
8-21-75	19:04:06.50	34.0575	106.9692	10	7.50	7.50
8-25-75	19:37:41.10	34.0714	106.9167	5	6.73	6.70
8-29-75	08:52:18.80	34.0737	106.9271	20	7.20	7.20
1-21-76	05:34:40.93	34.0630	106.9720	6	5.43	5.30
1-27-76	08:37:44.73	34.1290	106.8220	37	8.90	8.00
1-29-76	15:06:40.70	34.0000	106.9680	10	6.50	5.30
1-30-76	13:56:23.95	34.0690	106.9860	3	4.80	5.10
2-17-76	06:17:49.07	34.0450	107.0620	1	10.20	9.90
2-18-76	09:13:30.54	34.0183	107.0087	1	5.00	4.80
3-25-76	10:50:54.65	34.0425	106.9435	1	5.50	5.50
4-14-76	01:50:28.91	33.9910	106.9950	3	9.10	10.10
4-16-76	05:34:38.85	34.0380	107.0230	1	6.10	5.80
4-16-76	09:33:43.03	34.0670	107.0070	20	6.60	6.60

* km below the surface

h_1 depth from closest station

h_2 depth from iterative program

TABLE 5. (Continued)

Date	Origin Time	Latitude (°N)	Longitude (°N)	No. of Events	Depth* h_1	h_2
4-20-76	08:32:19.19	34.0980	106.8430	1	4.00	4.10
6-08-76	05:24:54.70	34.0606	106.9859	16	6.40	6.10
6-08-76	06:24:40.40	34.0565	106.9672	1	13.30	11.60
6-08-76	06:42:51.14	34.0626	106.9857	4	5.00	5.30

TABLE 6. Class G Events.

Date	Origin Time	Latitude (°N)	Longitude (°N)	No. of Events	Depth* h_1	Depth* h_2
5-20-75	14:25:09.20	33.9427	106.9488	2	--	5.0
5-20-75	17:10:01.60	34.0946	106.9144	2	--	9.4
5-22-75	10:27:08.50	34.0815	106.8794	1	--	4.0
5-22-75	11:36:29.03	33.9397	106.9395	1	--	4.7
5-26-75	23:45:51.30	34.0775	106.9810	1	--	8.0
5-29-75	07:14:12.12	33.9452	107.0168	1	--	8.0
6-03-75	02:45:09.60	34.0826	106.9062	12	--	3.3
6-03-75	04:48:17.80	34.0844	106.9204	1	--	9.3
6-16-75	23:43:21.11	34.0276	107.0242	1	7.80	10.8
6-17-75	15:30:45.14	34.0647	106.9129	2	9.10	7.3
6-17-75	18:50:33.31	34.0640	107.0520	2	--	10.6
6-26-75	02:56:45.11	34.0647	107.0365	2	--	6.1
7-01-75	13:35:58.50	34.0301	107.0408	2	--	9.9
7-09-75	02:12:24.80	34.0562	106.9302	6	--	6.1
7-09-75	09:16:47.97	34.0804	106.9167	1	--	8.7
7-24-75	04:23:14.30	34.0646	106.9940	1	--	5.2
7-30-75	21:44:42.10	34.0848	106.9223	1	--	8.2
8-05-75	02:26:02.50	34.0335	106.9772	8	--	7.6
8-05-75	04:17:20.92	34.0379	106.9839	1	13.00	7.8
8-07-75	09:04:30.60	34.4111	107.7232	1	--	13.0

* km below the surface

h_1 depth calculated from reflections

h_2 depth from iterative program

TABLE 6. (Continued).

Date	Origin Time	Latitude (°N)	Longitude (°N)	No. of Events	Depth* h_1	Depth* h_2
8-08-75	10:53:58.00	34.0837	106.9233	2	--	6.7
8-12-75	03:59:36.10	33.9574	106.9812	1	--	4.0
8-12-75	07:09:11.15	34.0357	106.8225	1	--	0.0
8-13-75	05:19:18.20	34.0823	106.9207	27	8.20	8.1
8-13-75	07:39:18.40	34.0826	106.9274	1	--	7.9
8-13-75	11:22:26.90	34.0245	106.9731	1	11.40	9.0
8-15-75	06:36:45.80	34.0871	106.8957	2	7.30	7.3
8-19-75	08:11:46.60	34.0580	106.9409	2	9.10	10.9
8-19-75	10:00:07.20	33.9922	107.0000	1	9.00	10.9
8-19-75	20:10:22.60	34.0971	106.9276	4	--	9.2
8-20-75	21:59:44.30	34.0947	106.9261	6	--	8.9
8-21-75	03:44:48.70	34.0407	107.0470	1	11.60	9.5
8-26-75	08:40:15.40	34.0480	106.9220	12	9.40	9.0
8-28-75	01:26:02.50	34.1264	106.9296	5	--	2.9
9-16-75	13:30:52.55	34.0804	106.9301	1	--	6.7
9-19-75	08:42:57.21	34.0234	106.8539	1	--	5.5
9-24-75	02:17:09.30	34.0954	106.9140	7	--	7.2
10-29-75	07:21:35.35	34.0609	106.9987	6	4.00	3.9
10-29-75	20:50:49.60	34.0134	106.9940	2	--	4.8
10-30-75	07:09:39.20	34.0335	107.0168	3	10.60	5.6
10-31-75	04:02:15.27	33.9345	106.7589	1	7.60	9.6
11-04-75	16:30:12.10	34.0491	107.0517	31	6.90	6.2
11-05-75	02:40:10.50	33.9973	106.7823	1	--	9.8
11-05-75	14:35:05.50	34.0402	107.0475	22	10.00	7.6

TABLE 6. (Continued).

Date	Origin Time	Latitude (°N)	Longitude (°N)	No. of Events	Depth* h_1	Depth* h_2
11-05-75	22:28:26.70	34.0424	107.0228	19	--	4.5
11-06-75	09:33:59.20	34.0396	107.0047	2	9.40	8.0
11-06-75	11:05:48.30	34.0078	106.8629	1	--	8.0
11-07-75	08:27:36.10	34.0480	107.0323	25	--	7.1
1-21-76	14:18:28.75	33.9840	106.9550	2	5.10	5.5
1-22-76	16:05:11.03	34.0450	107.0360	3	6.90	10.6
1-22-76	22:14:30.50	34.0340	106.9540	2	--	0.0
1-23-76	02:53:33.68	34.0280	107.0180	3	--	8.9
1-23-76	07:22:15.04	34.0620	107.0253	1	--	1.0
1-27-76	10:05:27.07	34.1490	106.8060	1	--	9.6
1-30-76	07:16:07.00	33.9970	106.9832	2	6.90	6.1
2-17-76	17:34:05.13	34.0520	107.0040	2	8.20	10.7
2-17-76	23:19:38.61	34.1110	107.0140	3	--	9.5
2-18-76	05:44:55.76	34.0240	107.0530	1	8.30	10.3
2-18-76	23:25:35.22	34.0420	107.0520	1	8.00	6.2
2-19-76	00:08:36.77	34.0260	107.0610	1	9.60	10.5
3-18-76	18:34:51.00	34.0420	107.0750	1	6.10	10.4
4-13-76	09:45:40.73	34.0720	107.0050	5	4.80	5.6
4-13-76	11:41:25.73	34.0450	107.0540	2	10.60	7.5
4-13-76	11:58:34.65	33.9900	106.9510	5	6.8	6.4
4-13-76	13:31:59.42	33.9840	107.0067	1	--	8.6
4-13-76	23:15:15.00	34.0300	107.0250	1	--	6.0
4-15-76	08:45:52.70	34.0680	107.0080	17	3.60	6.6
4-16-76	14:07:33.47	34.0686	107.0067	1	6.30	6.0

TABLE 6. (Continued).

Date	Origin Time	Latitude (°N)	Longitude (°N)	No. of Events	Depth* h1	Depth* h2
5-25-76	03:08:17.00	34.0452	107.0120	2	1.10	2.6
6-03-76	15:31:13:58	34.0374	106.9812	3	4.80	5.0
6-30-76	08:44:01.77	34.1241	107.0239	9	9.10	8.3
7-15-76	10:58:33.39	34.0480	107.0978	2	--	13.6
8-03-76	02:19:06.70	34.0679	107.0013	5	--	6.5
8-03-76	10:43:56.28	34.0573	107.0532	1	--	9.0
8-10-76	04:38:25.38	34.0197	107.0693	11	--	11.0
8-10-76	12:28:42.01	34.0622	106.9944	7	7.90	8.8
8-11-76	06:03:43.82	34.0571	106.9985	4	--	8.1
8-12-76	00:59:08.11	34.0563	106.9937	1	8.20	10.3
8-12-76	01:24:36.24	34.0638	106.9651	2	9.40	13.6
8-12-76	04:56:05.20	34.0548	106.9956	2	8.20	10.2
8-12-76	23:07:12.90	34.0558	106.9993	3	10.00	7.3
8-24-76	01:31:13.83	34.0498	107.0162	1	4.40	6.2
8-25-76	22:32:22.96	34.0571	106.9814	4	--	12.1
8-27-76	01:44:39.69	34.0544	106.9989	1	--	9.7
8-27-76	08:15:28.11	34.0174	107.0522	12	--	10.9
9-03-76	06:46:29.37	33.9772	106.9824	1	--	9.2
9-03-76	13:25:58.18	34.0070	106.9657	1	--	11.3

TABLE 7. Class B Events.

Date	Origin Time	Latitude (°N)	Longitude (°N)	No. of Events
4-17-75	00:02:18.40	34.2200	106.8800	4
4-17-75	17:31:07.70	33.9700	106.8700	2
5-20-75	10:34:23.30	33.9400	106.9400	1
5-20-75	13:20:40.00	34.2900	106.9300	1
5-22-75	13:19:41.40	33.9500	106.9400	1
6-03-75	04:03:00.70	34.0900	106.9900	1
6-04-75	04:20:14.20	34.0100	106.9400	1
6-17-75	00:00:54.10	34.0900	107.0200	1
6-17-75	02:19:53.90	33.9400	106.9400	1
6-24-75	20:47:34.50	34.3300	106.8800	1
7-02-75	01:00:19.25	34.2200	106.8800	2
7-03-75	16:12:20.90	34.0100	106.9700	1
7-09-75	07:55:42.20	34.2600	106.9000	1
7-22-75	00:29:19.20	34.2400	106.9500	1
7-22-75	22:45:34.50	34.0400	106.9600	3
7-24-75	17:10:14.25	34.0200	107.0300	1
7-27-75	18:50:19.20	34.2900	106.8700	1
8-01-75	11:26:20.90	34.0800	107.0200	1
8-05-75	14:19:22.13	34.0700	107.0500	2
8-06-75	20:12:33.20	34.0300	106.9700	1
8-13-75	05:29:49.48	34.2000	107.0400	1
8-14-75	05:16:15.10	34.2900	106.8900	1
8-14-75	19:03:28.30	34.1000	106.9300	5
8-15-75	07:33:52.40	34.0200	106.9600	3

TABLE 7. (Continued).

Date	Origin Time	Latitude (°N)	Longitude (°N)	No. of Events
8-19-75	02:14:21.60	34.2100	106.8900	1
8-22-75	00:34:05.60	34.0300	106.9700	1
8-27-75	07:35:13.20	34.0900	106.9300	8
10-24-75	10:54:17.00	34.3900	106.8900	12
11-29-75	09:34:37.10	34.0500	107.0000	1
11-29-75	09:18:23.60	34.0600	107.0000	1
1-22-76	12:16:08.80	34.4057	107.0198	1
1-22-76	22:50:07.60	34.1770	106.8830	1
2-05-76	19:45:32.30	34.4985	107.0248	1
2-06-76	09:20:58.40	34.3222	106.9930	1
2-19-76	00:54:42.60	34.5016	107.0405	1
2-20-76	12:51:45.10	34.0310	107.0450	2
3-18-76	14:45:16.00	33.9760	106.7260	11
3-23-76	12:50:26.35	33.9800	106.7050	1
3-23-76	12:53:20.55	34.2500	106.8370	1
3-24-76	22:52:17.75	33.9722	106.7232	1
3-25-76	13:57:02.90	34.0430	107.0660	1
4-14-76	13:12:21.50	34.0710	107.0310	2
4-20-76	02:52:19.33	34.0470	107.0620	1
4-21-76	11:16:20.17	34.2880	106.8530	2
4-22-76	04:18:07.10	33.9670	106.7310	1
4-23-76	05:57:59.97	34.0600	107.0390	2
5-25-76	08:11:38.95	34.0322	107.0682	3
5-26-76	19:54:19.24	33.9428	106.7896	1

TABLE 7. (Continued).

Date	Origin Time	Latitude (°N)	Longitude (°N)	No. of Events
6-01-76	08:38:47.75	34.0258	107.0537	1
6-09-76	17:36:46.35	34.4090	106.9259	1
7-02-76	00:28:09.04	34.1743	106.9234	1
7-14-76	21:22:55.05	34.0088	107.0173	1
7-15-76	16:43:07.60	34.0269	107.0578	3
7-28-76	12:14:48.51	34.4316	106.9973	1
7-28-76	12:39:00.49	34.1191	106.7538	1
7-30-76	11:11:40.20	34.4534	107.5823	1
8-03-76	07:10:15.20	34.4907	106.9767	1
8-09-76	23:08:14.70	34.4567	107.0093	1
8-11-76	03:15:19.20	34.1547	106.8756	1
9-02-76	12:51:37.93	34.1538	106.8780	1
9-03-76	09:13:02.53	34.1496	106.8745	1
9-03-76	15:29:26.61	34.1223	106.9745	1

SPATIAL DISTRIBUTION OF MICROEARTHQUAKES

Tables 5, 6, and 7 list origin times and hypocenters for 163 microearthquakes that occurred from May, 1975, to September, 1976. Because swarms of earthquakes from the same hypocenter are common in the Socorro area, the 163 locations in these tables are the hypocenters for a total of 645 individual shocks. The number of shocks associated with each hypocenter listed is given in column 5 of Tables 5, 6, and 7. About 70 percent of all shocks during the study occurred in swarms.

Figure 4 shows the location of epicenters with respect to surrounding surface features. The general geographical distribution can be described as diffuse with a fairly broad band of activity extending along the axis of the Rio Grande rift. Pockets of activity occur 3 km northeast of WT; 4 km southwest of WT; and 10 km southwest of WT. The distribution of activity in Figure 4 is similar to that obtained in other periods of microearthquake monitoring. The majority of microearthquake activity has not been associated with the major frontal faults of the intergraben horsts (Sanford and Holmes, 1962; Sanford, 1963; Sanford and others, 1972).

Depths of focus were found to range from the surface to 13.3 km below the surface. Approximately 60 percent of the events occurred between 6 and 9 km below the surface.

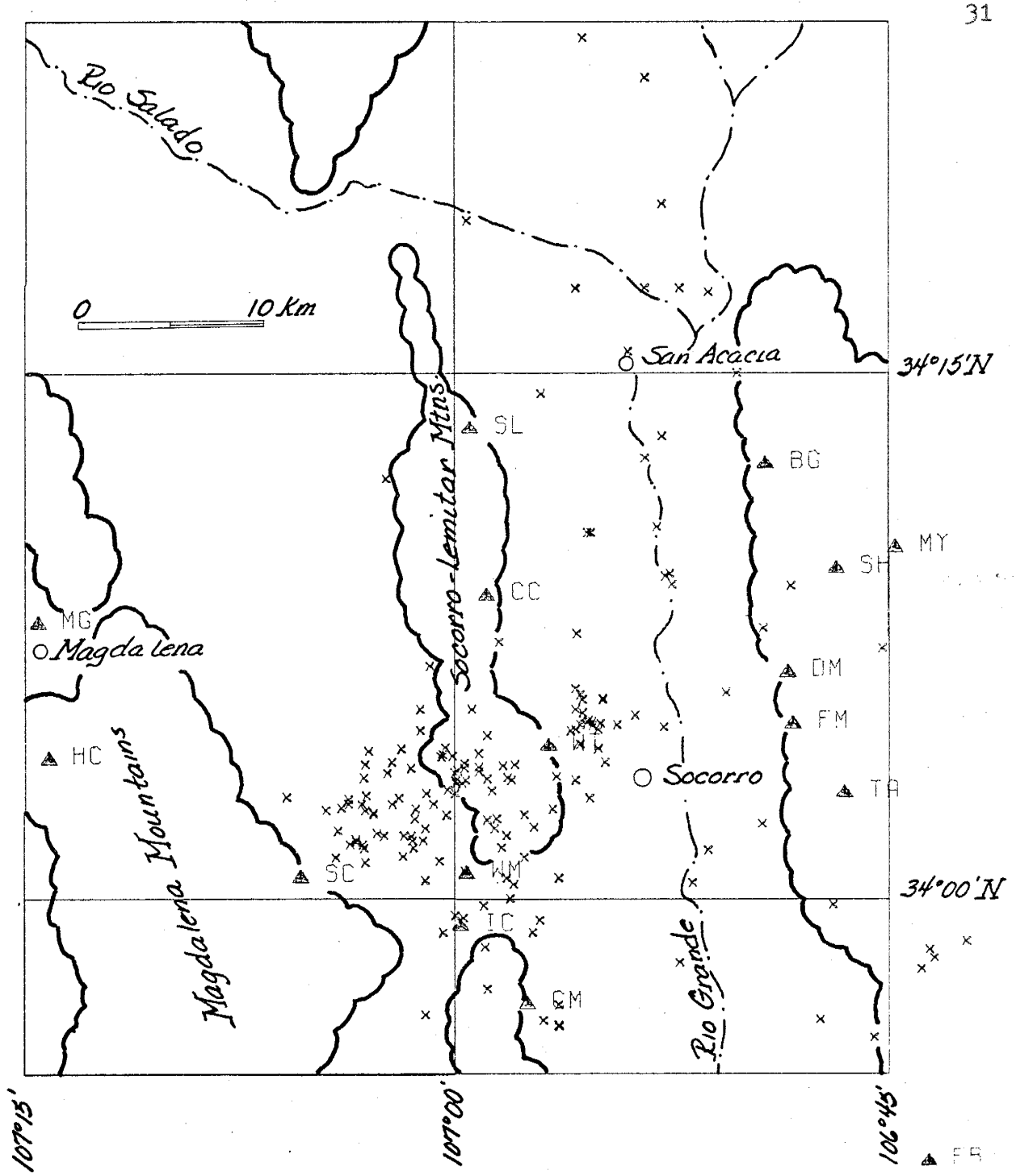

Figure 4. Locations of microearthquakes with respect to surface features.

THE MAGMA LAYER

1. Introduction

From previous studies (Sanford and Long, 1965; Sanford and others, 1973), the existence of an extensive magma body approximately 18 km beneath Socorro has been known for several years. A primary effort of this study was to map, with some confidence and resolution, the lateral extent and relief of this body. The microearthquake reflection data in this report were sufficient to achieve these goals along the southern margin of this body.

Calculations of depths to reflector and reflection points were made by using the following equation (see Figure 5):

$$(2Z - h)^2 = (S_ZS \cdot V_S)^2 - \Delta^2$$

$$\text{or} \qquad Z = \frac{h}{2} + \left\{ \frac{(S_ZS \cdot V_S)^2 - \Delta^2}{4} \right\}^{1/2}, \qquad (1)$$

$$\text{and} \qquad A = \text{TAN}(R) \cdot (Z - h), \qquad (2)$$

where Z is the depth to the reflector and A is the horizontal distance from the epicenter to the point of reflection. These same equations, using a known reflector depth, were used to find hypothetical points of reflection for events not having actual S_ZS reflection phases, and also to calculate depths of focus for the Class G events.

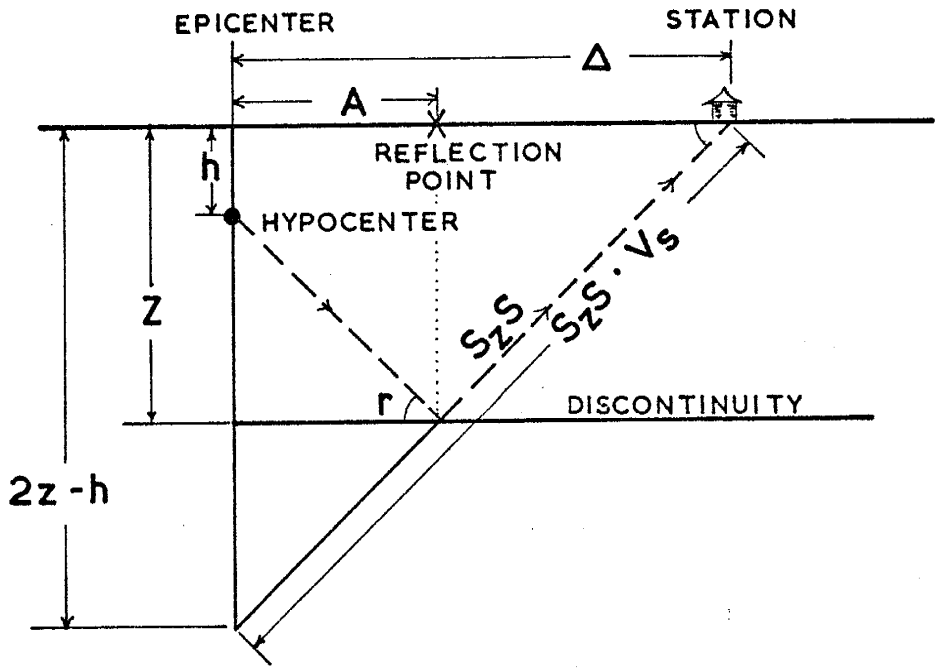

Figure 5. Cross section of the crust showing ray paths and distances used in calculating the depth of the magma layer.

2. Lateral Extent of Magma

All S_ZS arrival times, measured with an accuracy of $\pm$0.1 second, from all three classes of events were used to calculate the geographic location of reflection points shown in Figure 6. The lack of reflection points in Figure 6 could be due to either an absence of the reflective surface or a lack of data. To find out which of these options was true, hypothetical reflection points were calculated for all events without S_ZS phases. Hypothetical reflection points, shown in Figure 7, were calculated assuming an 18 km discontinuity for the entire area.

A comparison of Figures 6 and 7 indicates ample opportunity for S_ZS reflections from certain areas, yet no true reflections were detected. Thus the boundary in these regions could be mapped with some assurance. The boundary is highly irregular with some areas of no reflections being almost surrounded by the magma body.

North of 34.12°N the distribution of hypothetical reflection points along with true reflection points was inadequate to accurately define the margins of the body. However, the data were sufficient to establish a minimum extent in these areas. If information from Sanford and others (1973) is included, the minimum areal extent of the body is about 1200 km^2. The magma body follows the general trend of the Rio Grande Rift, with its margins never extending beyond the boundaries of the rift.

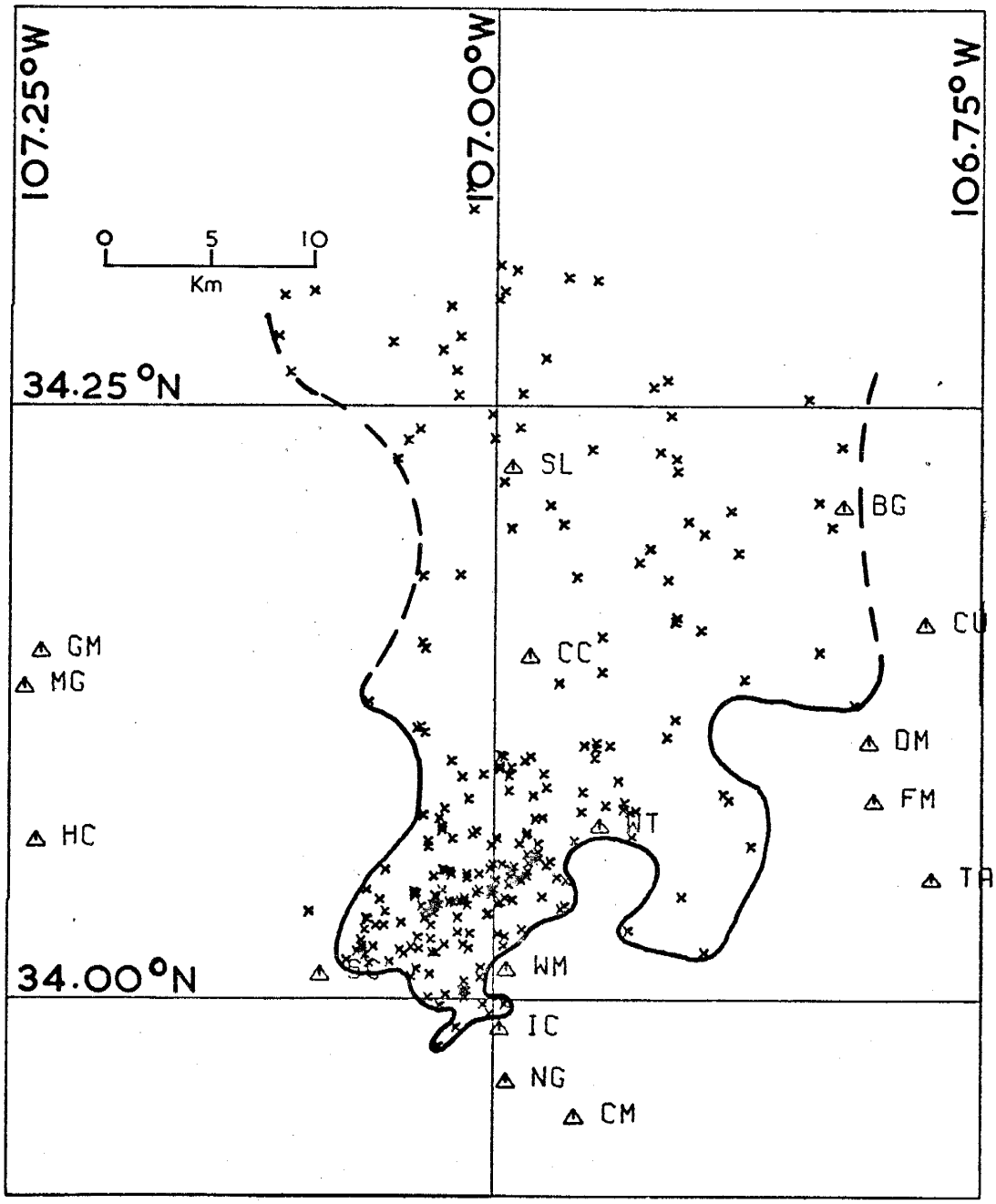

Figure 6. Points of reflection. Data was obtained from May, 1975, to September, 1976.

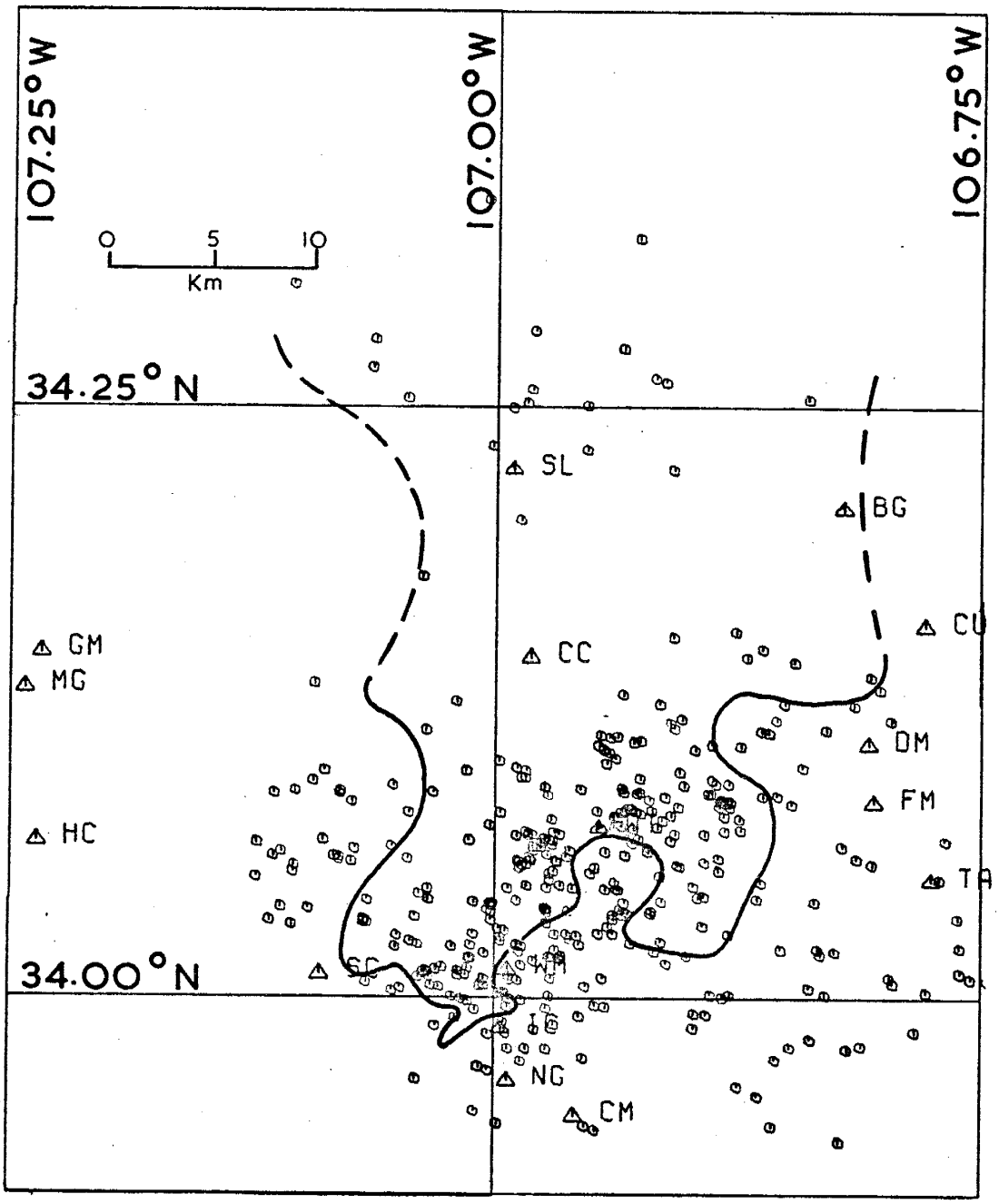

Figure 7. Hypothetical points of reflection. Data was obtained from May, 1975, to September, 1976.

To find out how accurately the coordinates of each reflection point were determined, the depth of focus, origin time and S_ZS - P times for the event occurring on 01-21-76 at 05:34:40.93 were incremently changed from their true values. The depth of focus was changed from 2 km to 10 km, at 1 km steps; the origin time was changed from +0.1 second of the true origin time to -0.4 second, at 0.1 second steps; and the S_ZS - P time was changed by 0.4 second. For all introduced perturbations of the data, the lateral changes in the reflection point did not exceed $\pm$1.5 km. Because the lateral error was small, even for large errors in depth of focus, Class B events were also used in mapping the areal extent of the body.

Equation (1) shows that determination of the relief on the magma body requires precise depths of focus which, unfortunately, are the least accurately determined hypocentral coordinates. Equation (1) also indicates that any error in the depth of focus would be halved when calculating a depth to the discontinuity.

To get good depth control of the magma body, only Class E events were used initially. The surface calculated from these events was used to obtain more accurate depths of focus for Class G events which had S_ZS arrivals. If a Class G event had two or more stations that received S_ZS reflections, the reflection arrival time for the nearest station was used to determine a new depth of focus. Reflection arrivals at other stations were then used with the new depth of focus to determine a depth to the magma body. The new depths of focus for Class G events are listed in column 6 of Table 6.

Both north-south cross sections and east-west cross sections (see Figure 8) of the depth values were constructed using both Class E and Class G data. The actual relief on the magma surface was obtained by drawing smoothed profiles through the depth points of the cross section. A three-dimensional computer plot of the results is shown in Figure 9. Total relief is about 2 km with depths ranging from about 18 km to 20 km below the surface. The magma body appears to have a NS ridge roughly aligned with the intergraben horst (Socorro Mountains) in the center. The deepest regions of the magma body are along the western and southern margins.

3. Physical Properties of the Discontinuity.

Sanford and others (1973) concluded that abnormal amplitude ratios of S_ZP to S_ZS were due to rock of very low rigidity underlying the discontinuity. They also concluded that the high frequency content (15 to 20 Hz) of the reflections indicated a sharp discontinuity, i.e. a transistion zone only 10's of meters thick. Although a sharp discontinuity underlain by magma was a reasonable interpretation of the data, the observations could possibly have been explained in an alternate manner. Berryman and others (1958) showed that a multilayered section with thin layers could also produce strong, high frequency reflections; however, the resulting reflections would contain very little low frequency energy.

A study was undertaken to determine if the S_ZS signals contained low frequency energy. Earthquake swarms were ideal for this study because small shocks within the swarms were

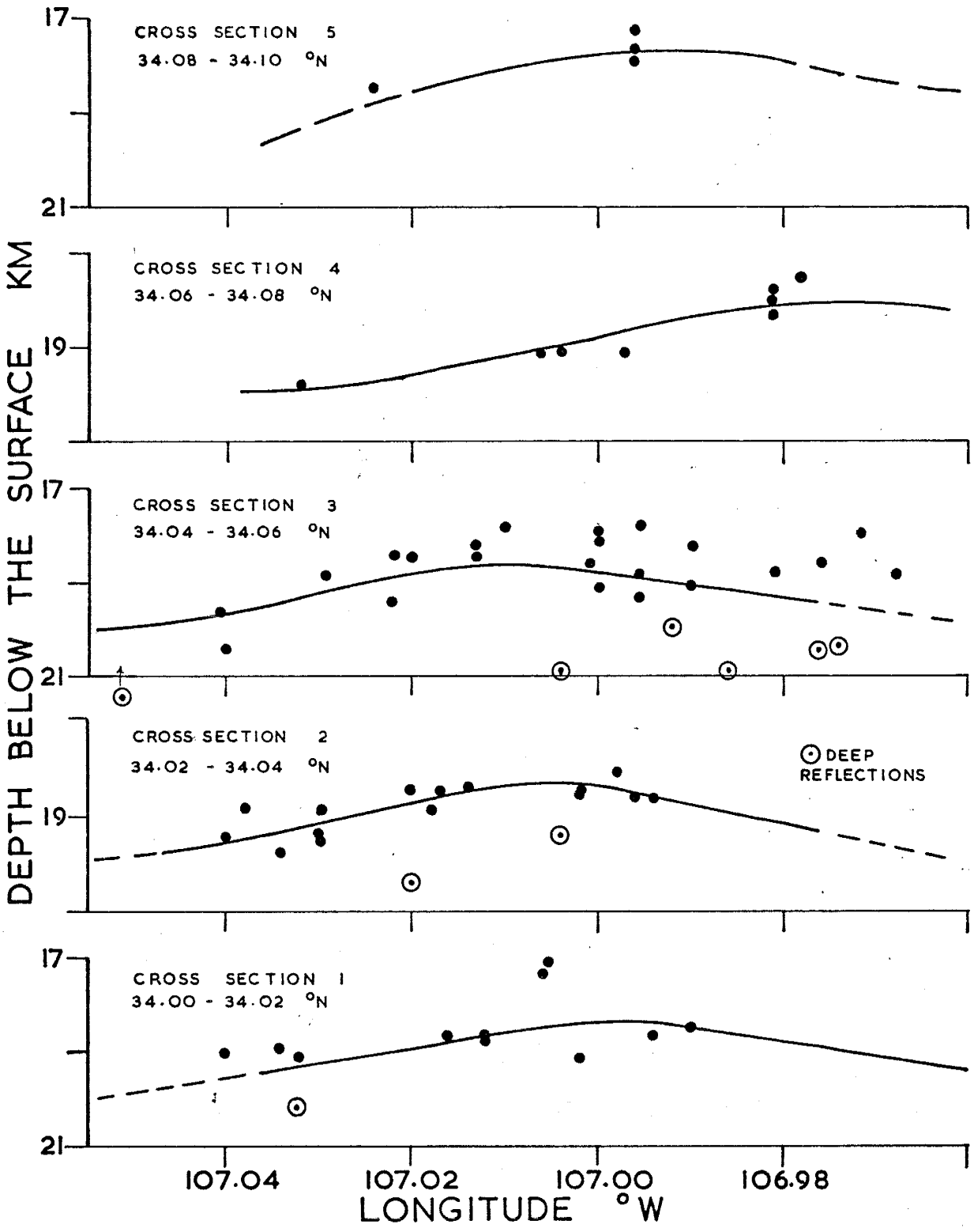

Figure 8. East-west cross sections of the magma body.

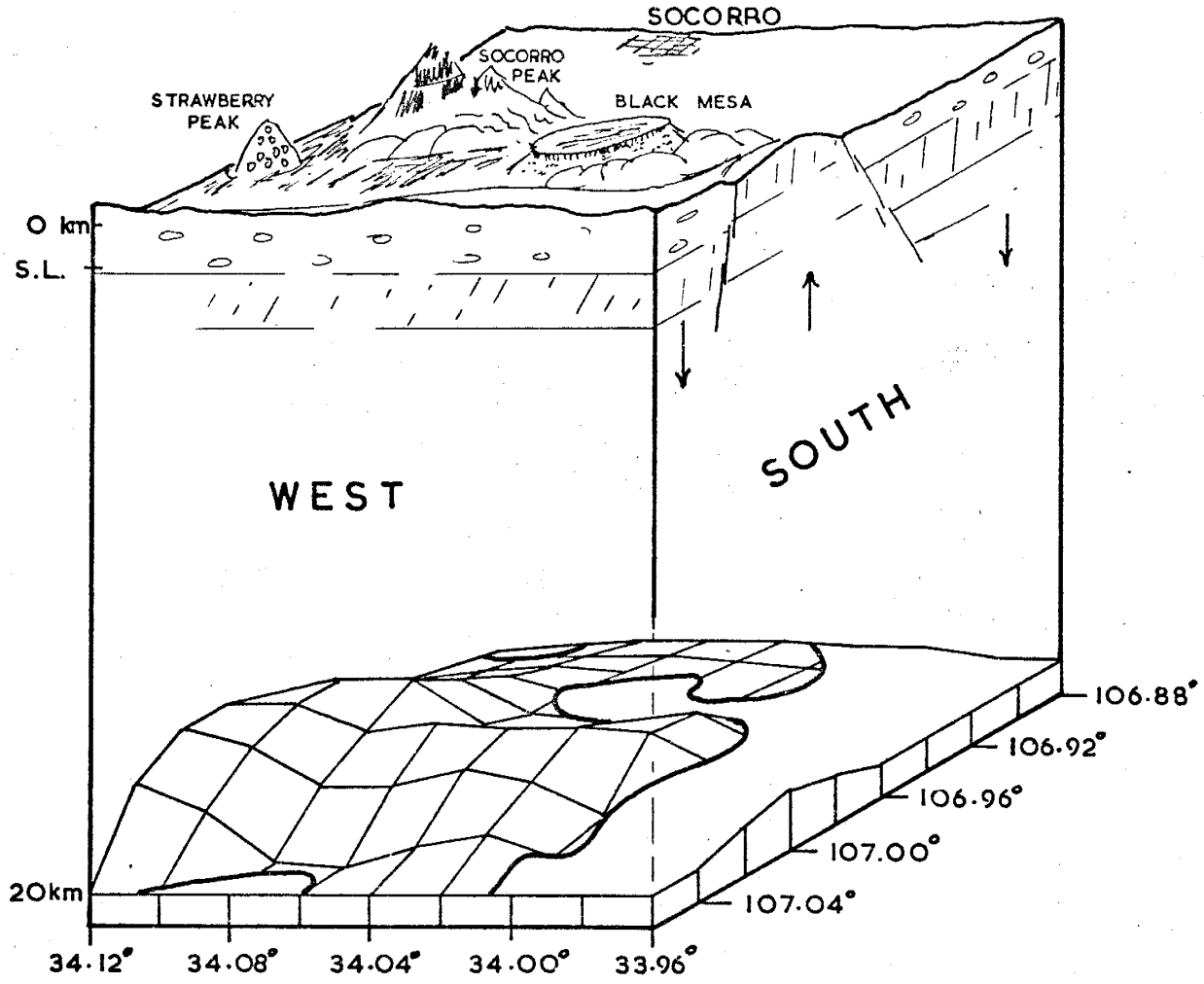

Figure 9. Computer generated three-dimensional plot of the magma body based on data from both Class E and Class G events.

recorded without signal saturation on the MEQ-800 seismographs, a system with good high and low frequency response. Large shocks within the swarms were recorded well on the LRSM system which does not have good high-frequency response.

Seismograms from microearthquakes swarms recorded on both the LRSM system at SNM and a MEQ-800 located at WT are shown in Plate 1. Both sets of seismograms, one for the LRSM and the other for the MEQ-800, show strong S_ZS reflections; however, the frequency content for both sets of data are noticeably different. The dominate frequency for the LRSM records is about 3 Hz while that of the MEQ-800 is about 15 Hz. Plate 1 also indicates that a lower frequency component appears in the SzS reflections on the MEQ-800 record. The mere existance of this low frequency content in the S_ZS reflections rules out a multilayered section with thin layers.

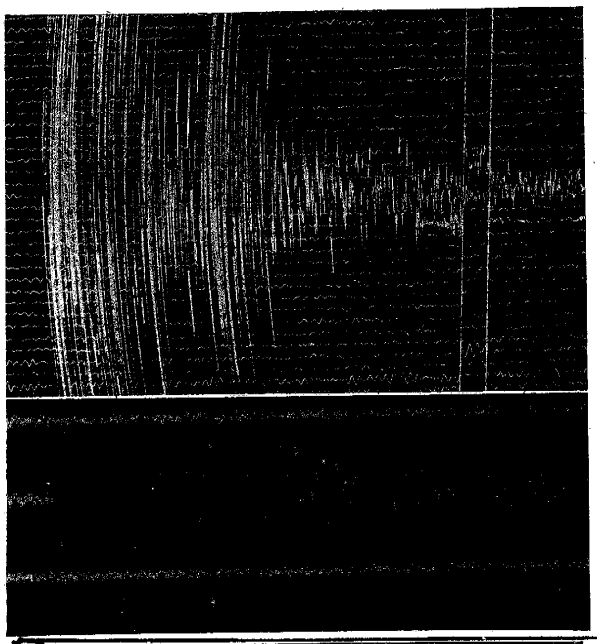

MEQ-800

LRSM (HORZ)

Date: 08-12-76

Time: 01:45

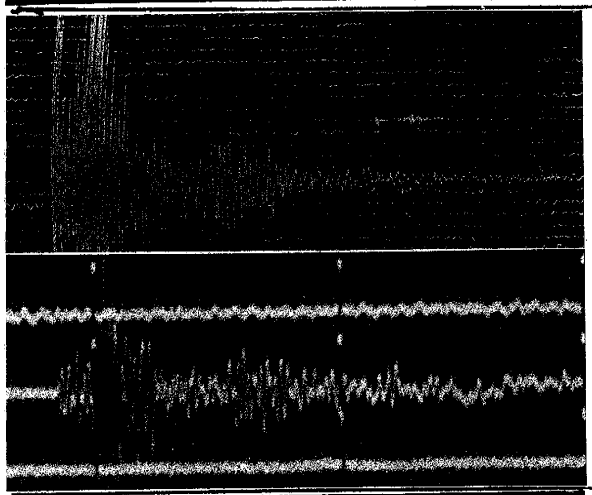

MEQ-800

LRSM (HORZ)

Date: 08-12-76

Time: 07:52

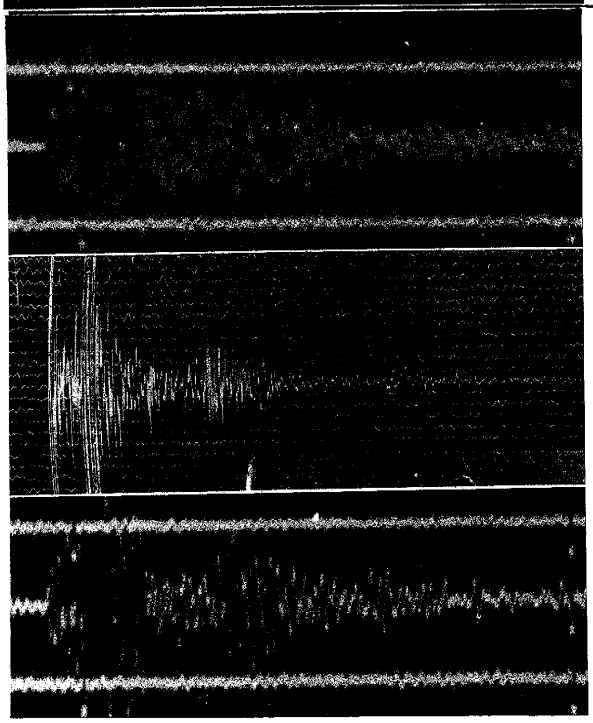

LRSM (VERT)

MEQ-800

LRSM (HORZ)

Date: 08-12-76

Time: 00:23

0 10 20

Seconds

Plate 1. Seismograms of microearthquakes recorded on both the LRSM system at SNM and a MEQ-800 field unit at WT.

DISCUSSION

1. Distribution of Locations

Two general geophysical observations suggest that the magma body at 18 km is undergoing inflation. The first is the level line data (Reilinger and Oliver, 1976) that indicates surface uplift above the magma body. The second observation is the distribution of microearthquakes, both in time and space.

Approximately 70 percent of the activity in this study occurred in swarms; swarms being defined as 5 or more events occurring within 12 hours from the same hypocenter. Figure 10 shows the distribution of these swarms from May, 1975, to September, 1976. Most of the swarm activity occurred over the known extent of the magma body.

Earthquake swarms have been observed in the areas of active volcanoes and areas that have had geologically recent volcanic activity (Richter, p. 71, 1958). It also is believed by some that intrusion at shallow depths of magma was the primary cause of the earthquake swarm near Matushiro, Japan (Stuart and Johnston, 1975).

The distribution of swarms of earthquakes at Socorro suggests that magma is being actively injected into the 18 km deep magma reservoir. The southerly positioning of these swarms also suggests that the magma body is trying to extend itself southward.

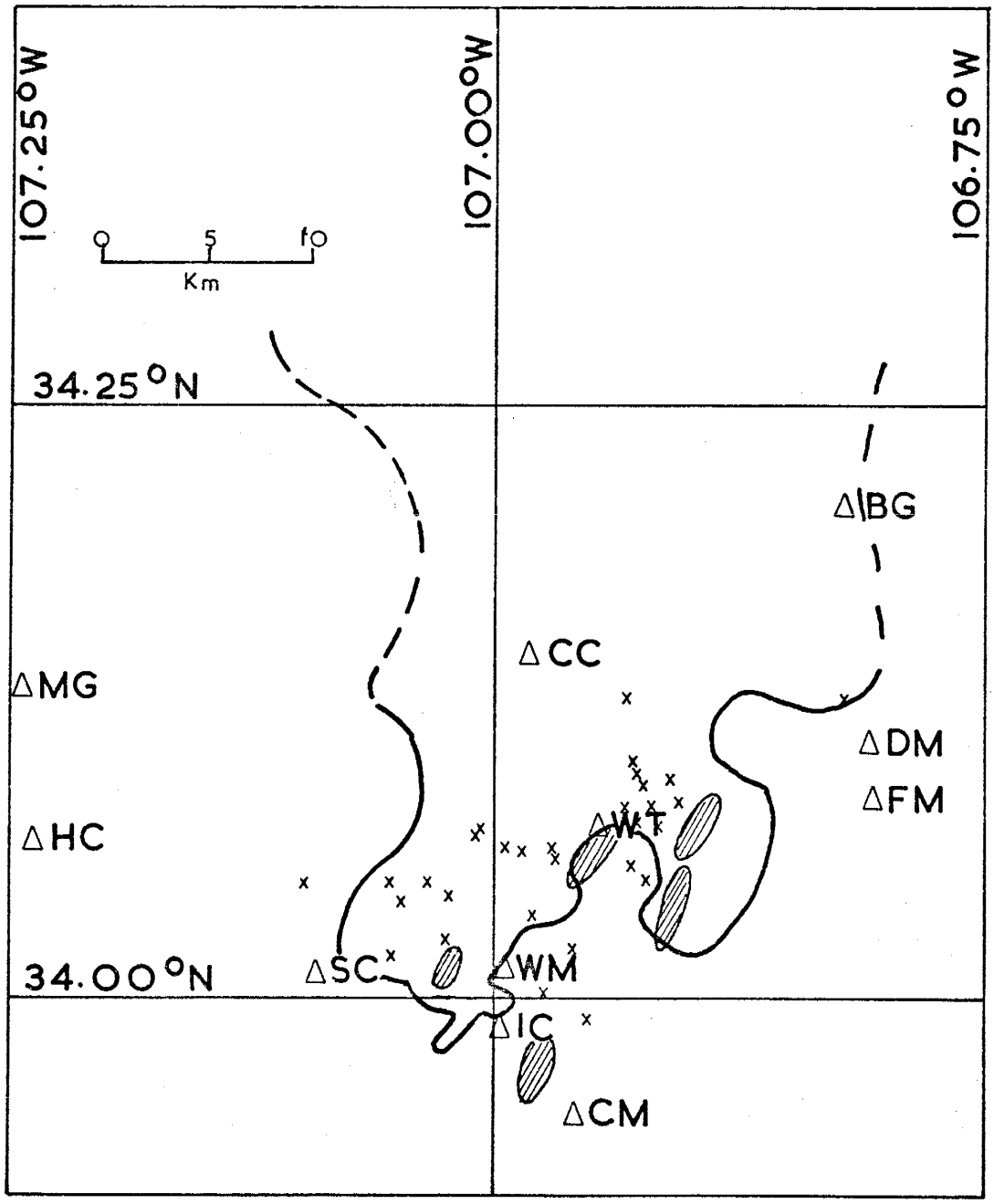

Figure 10. Location of all swarms in the Socorro area from May, 1975, to September, 1976, with respect to the extensive magma body and the shallow magma bodies proposed by Shuleski (1976)

All of the swarms outside the boundaries of the extensive magma body, except one, are located between stations WT and CM. Swarms in this region may be in some way related to the proposed shallow magma bodies (Shuleski, 1976) that surround the area (see Figure 10).

Figure 11 shows all independent microearthquake epicenters with respect to the extensive magma body for the period May, 1975, to September, 1976. The general distribution can be described as diffuse. Considering the numerous known major faults in the area (see Sanford and others, 1972), one might have expected the activity to be aligned along certain of these faults, especially the ones bordering the rift.

The rift is an extensional feature formed by a stress field having a maximum compressive stress in the vertical direction and a minimum compressional stress in the east-west direction (Chapin and Seager, 1975, and Sanford, 1968). Fault-plane solutions of 69 microearthquakes (Shuleski, 1976) indicate that nearly all microearthquakes are the result of the same stress field.

An effect of the inflation of the extensive magma body would be an uplift and a decrease of horizontal compressive stress along the axis of the uplift. If the direction of the new tensile stress coincided with the existing east-west least compressive stress, the probability of seismic slip would be enhanced. This slip would not necessarily be identified with any particular pre-existing fault system and could produce the diffuse pattern of activity found in the Socorro area. Stuart

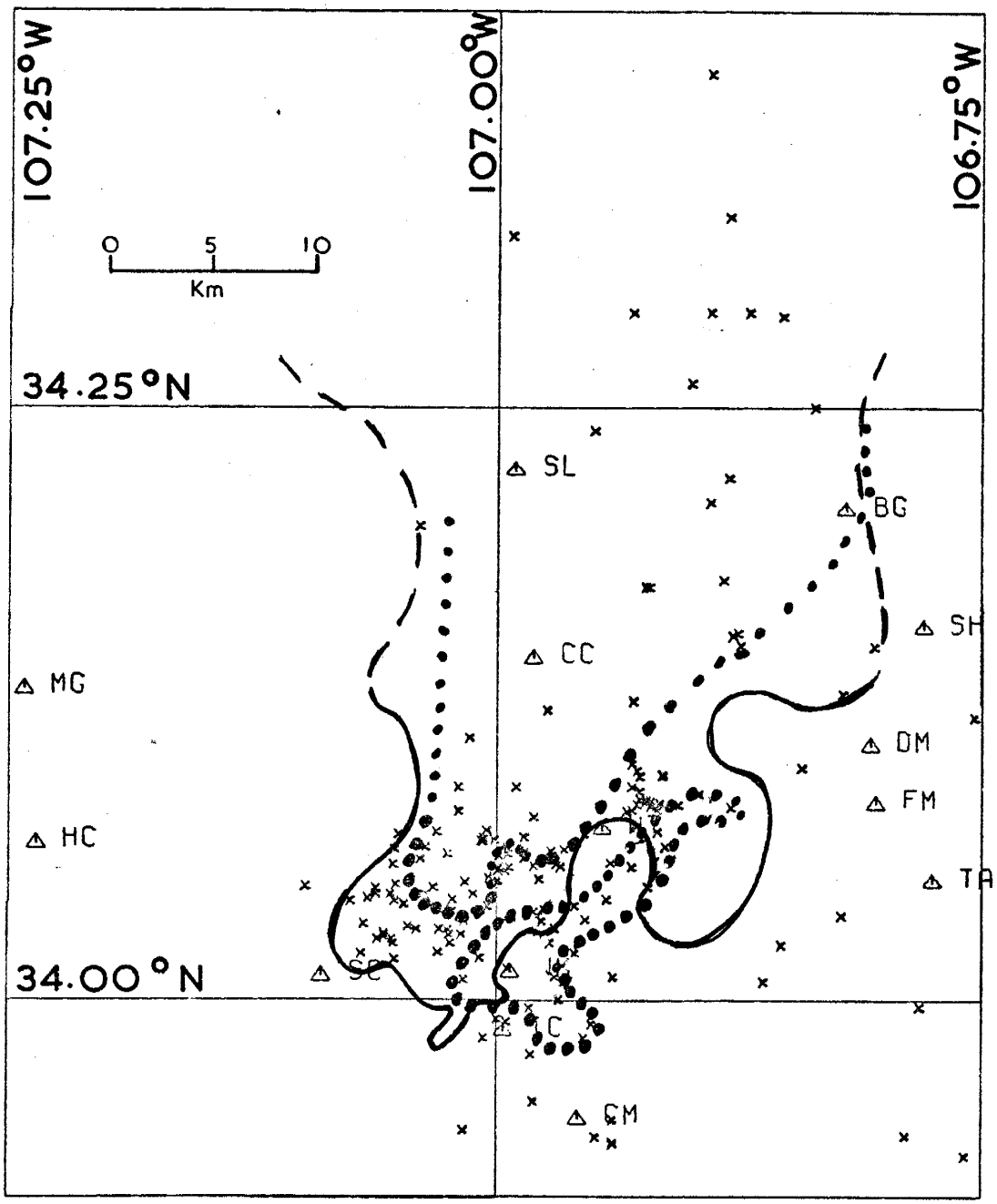

Figure 11. Location of microearthquakes with respect to the extensive magma body. Areas of shallow focus (< 8 km) events are surrounded by dots. All other areas contain events with depths of focus from 0 to 13.3 km.

and Johnston (1975) have used similar stress models to explain the diffuse activity of the Matushiro swarm.

A histogram (see Figure 12) of depths of focus reveals a possible bimodal distribution--one group of events with depths less than 8 km below the surface, the other with depths greater than 8 km below the surface. The largest area containing only shallow focus events (see Figure 13) is well within the margins of the extensive magma layer. The second area of shallow events is in the area between stations WT and CM. All other areas contain a mixture of both deep and shallow shocks. These mixed areas are gernerally located near the southern margin of the extensive magma body.

Three explanations for the distribution of the depths of focus are postulated:

(1) Some time after the magma was injected, the deeper rock (at depths greater than 8 km) became heated and more prone to creep rather than fracture. This could account for the central areas of shallow shocks.

(2) The area of shallow events between stations WT and CM is surrounded by the shallow magma bodies proposed by Shuleski (1976)(see Figure 13). These shallow magma bodies may influence the physical properties of the surrounding rock enough to permit no deep focus events.

(3) The deeper events along the southern end of the magma body could be a result of the southerly extension of the magma into cooler rock.

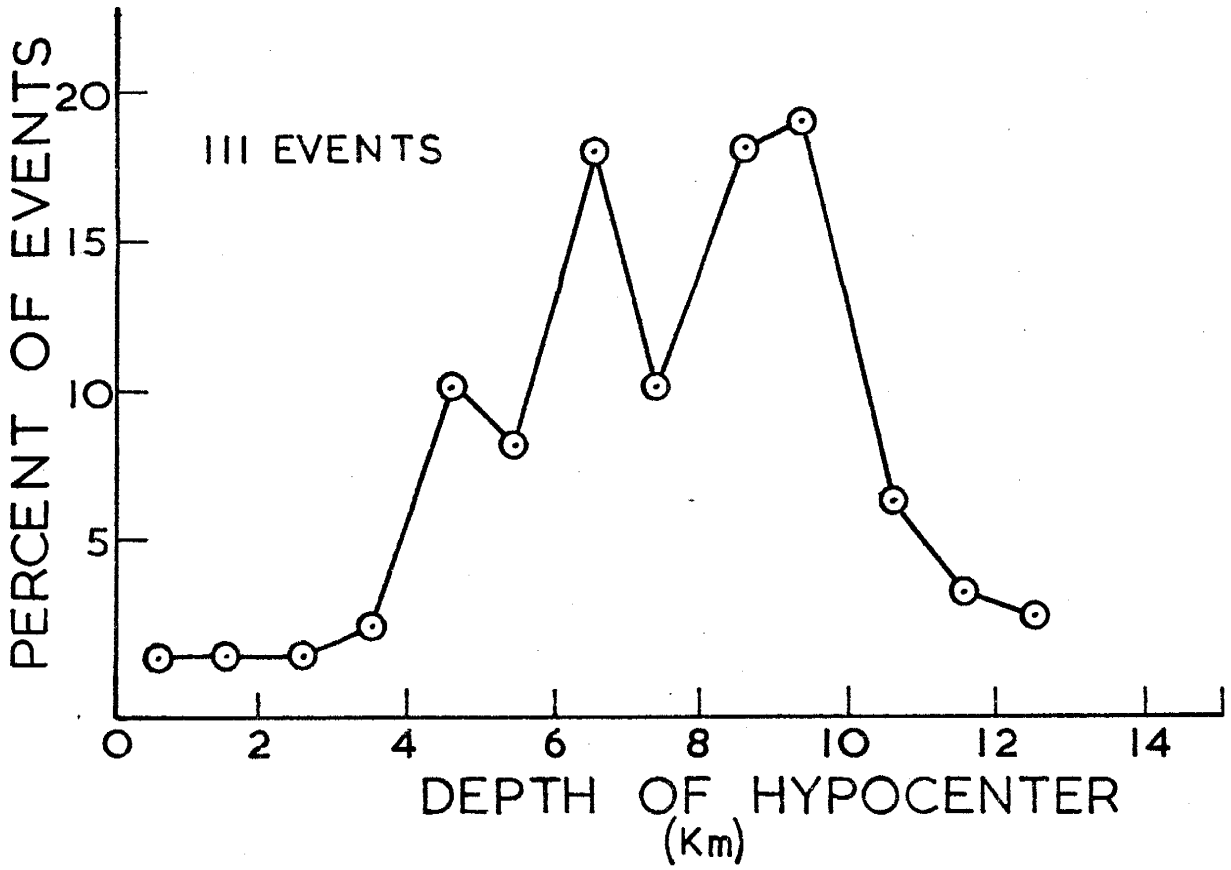

Figure 12. Histogram of depths of focus for Class E and Class G events.

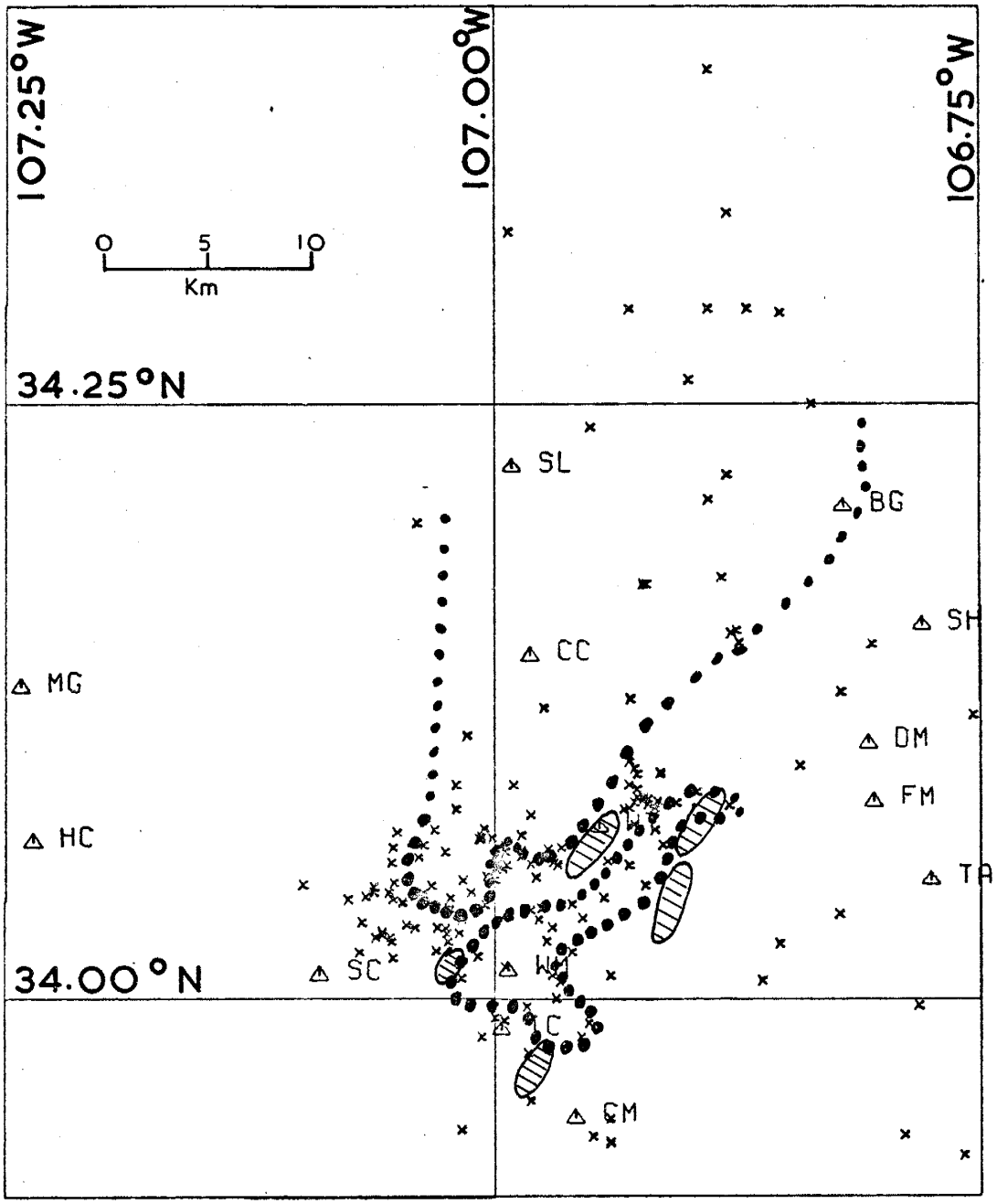

Figure 13. Areas of shallow focus (< 8 km) events (surrounded by dots) with respect to the shallow magma bodies proposed by Shuleski (1976)(hatched areas).

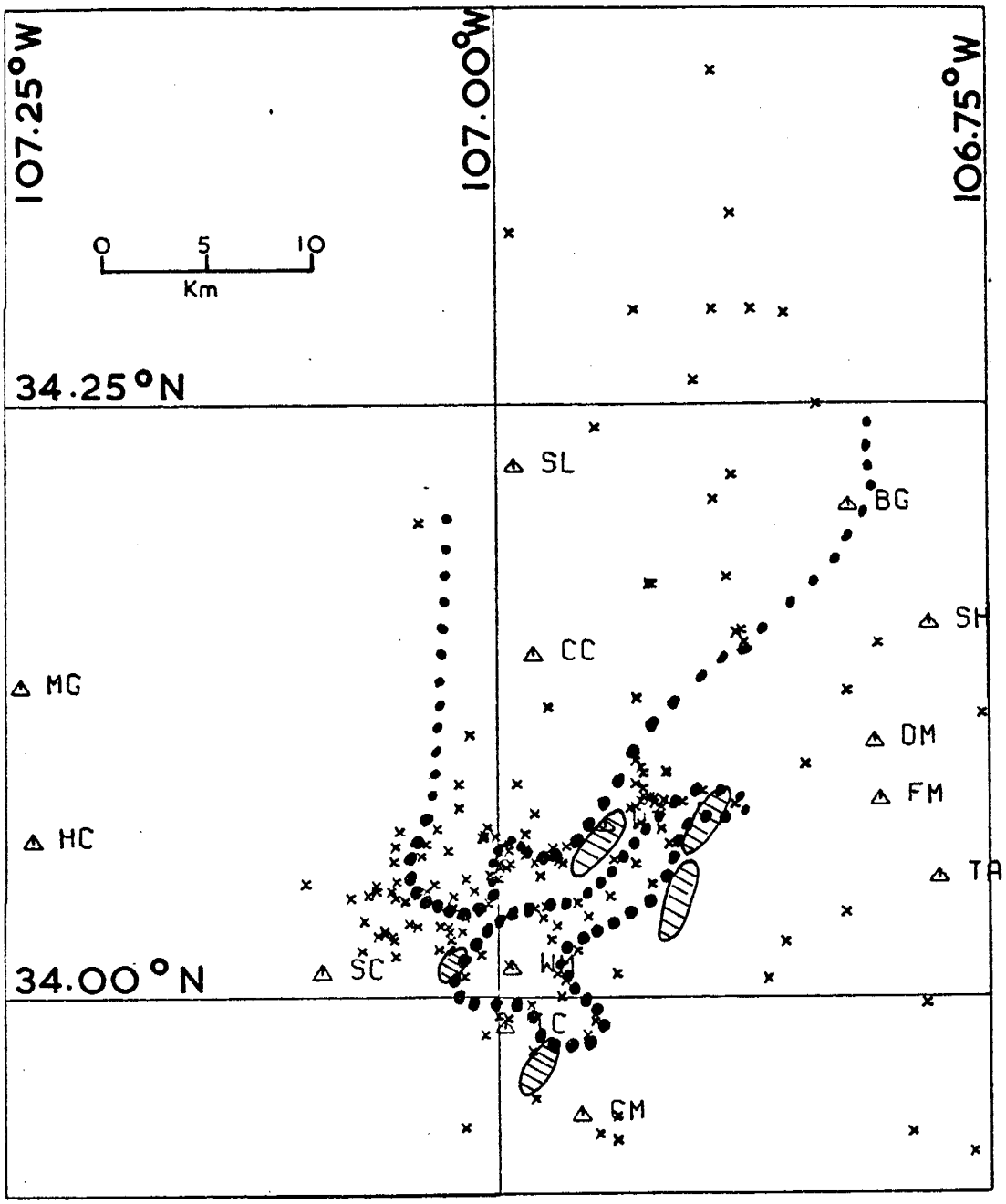

Figure 13. Areas of shallow focus (< 8 km) events (surrounded by dots) with respect to the shallow magma bodies proposed by Shuleski (1976)(hatched areas).

The above hypotheses are highly speculative. The lack of deep events in certain areas may only be due to an inadequate data set.

2. Extensive Magma Body at 18 Km.

The depths of focus for all events used in determining the relief of the discontinuity were known to within ±2 km and thus a scatter of ±1 km in depths to the discontinuity was expected. However, Figure 8, especially cross section 3, reveals several data points outside of the expected scatter. These data have depths of up to 2.5 km deeper than the proposed discontinuity. These deeper points would correspond to depths of focus errors of up to 5 km. Inasmuch as this large an error is unlikely, a time delay of the S_ZS reflections appears probable. The shallow magma bodies suggested by Shuleski (1976) might produce these time delays. The S_ZS reflections could be passing through areas of partial melt which would have low S wave velocities. This explanation is plausible considering that many of the deep data points do occur in an area containing two of the proposed shallow magma bodies (compare Figures 8 and 11).

If delay times do exist for the S_ZS travel times, complete absence of many of them could also be possible through shear wave screening by magma. Table 8 lists the percentage of microearthquakes witnessed at 8 stations. There are considerable differences in the number of reflections recorded at each station which suggests that some sort of mechanism is preventing certain stations from receiving all possible S_ZS

reflections. Also included in Table 8 are the percentage of microearthquakes with small SV wave amplitudes (Shuleski, 1976). The order of both sets of data is exactly the same, possibly suggesting that the amplitudes of SV waves and S_ZS reflections were reduced by the same mechanism. Only 40 percent of the weak SV wave could be explained by fault mechanisms of the microearthquakes; the other 60 percent were explained by S wave screening (Shuleski, 1976). Assuming that these percentages hold true for the reflections, S_ZS screening could be real.

Two very small areas, shown in Figure 14, produced no true reflections, although many possibilities did exist (see Figure 7). These two areas are in close proximity of two proposed shallow magma bodies. The absence of reflections could possibly be associated with S_ZS screening by the two shallow magma bodies.

TABLE 8. Percentages of Microearthquakes Having Weak S_ZS Reflections and Small W_e/W_S Amplitude Ratios at Seismograph Stations.

Station	Percentage of Microearthquakes with Weak or No S_ZS Reflections	Percentage of Microearthquakes with Small(1.5) Wp/W_S Amplitude Ratios
CC	33	0
SC	40	12
WT	53	27
WM	58	33
IC	62	33
DM*	82	38
FM*	85	66
TA*	87	78

* The low percentage of S_ZS reflections at these stations could be caused by the absence of a reflective layer on the eastern side of the rift.

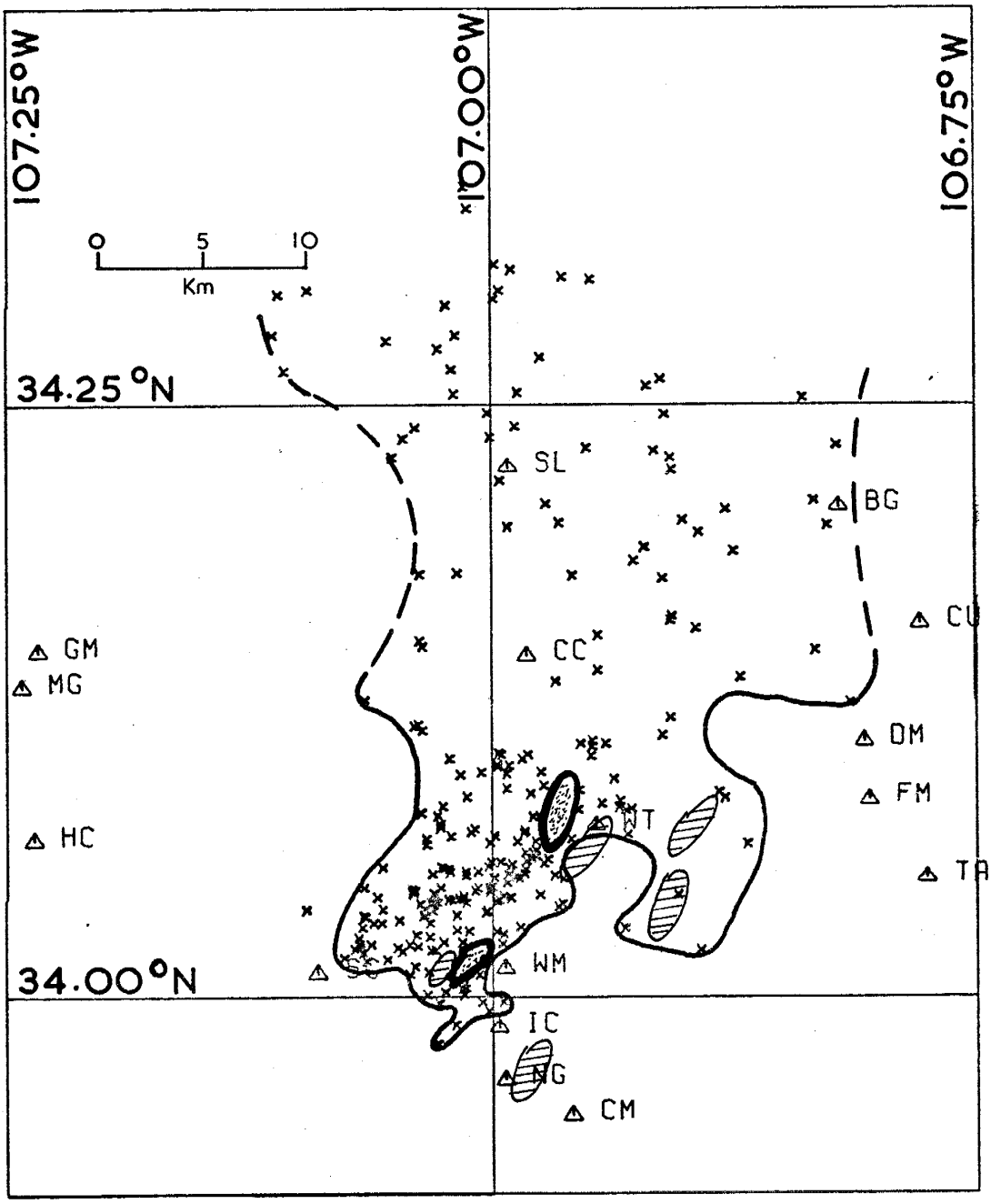

Figure 14. Small areas containing no reflection points (dotted areas) with respect to the proposed shallow magma bodies (Shuleski, 1976) (hatched areas) and the extensive magma body.

FUTURE STUDIES

Much more work is needed to determine the amount of S_ZS reflection screening by shallow magma bodies. The large area below station WT, which is surrounded by shallow magma bodies, may actually contain the 18 km discontinuity; however, all evidence of it may have been screened by the bodies. By calculating actual travel paths of specific S_ZS phases, perhaps particular volumes could be identified as causing the screening. The procedure would be similar to that followed by Kubota and Berg (1968) or Matumoto (1971).

At this time P wave velocities for the upper crust are beginning to be determined through the inversion of travel time data from local microearthquakes. Although a valuable aid to modeling the crust, it is only useful for crustal volumes above the foci. It may be possible to sample the crust as deep as 18 km by inverting both S_ZS and S_ZP data. This inversion could also identify areas with low S wave velocities or high Poisson's ratios (areas of partial melt).

Because anomalous frequency and amplitude attenuation occur in partially melted areas, these two characteristics should be investigated. The crust could be subdivided into prisms and the anomolous areas identified by inverting the attenuation data. This would, of course, require a great deal of digitized data that was unavailable in this study.

Up to this time the only detailed information about the extensive magma body has been obtained along the southern margin. Extensive data collection north of 34.12°N is necessary to fully map the discontinuity.

ACKNOWLEDGEMENTS

I would like to extend my sincere appreciation to Dr. Allan Sanford for his many hours spent in all areas of this research. His critical review of this paper is also appreciated. Gratitude is also extended to Richard Mott, Paul Shuleski, Terry Wallace and Frank Caravella for their help in data collection and reduction. Hypocenters were found by Roger Ward's iterative computer code.

REFERENCES CITED

Berryman, L. H., P. L. Goupillaud, and K. H. Waters (1958). Reflections from multiple transition layers, Part I--Theoretical results, Geophysics, XXIII, 2, 223-243.

Chapin, C. E. and W. R. Seager (1975). Evolution of the Rio Grande Rift in the Socorro and Las Cruces area, in New Mexico Geol. Soc. Guidebook, 26th. Field Conf., 297-321.

Kubota, A. and E. Berg (1968). Evidence for magma in the Katmai Volcanic range, Bull. Voc. 31, 195-214.

Matumoto, T. (1971). Seismic body waves observed in the vicinity of Mt. Katmai, Alaska, and evidence for the existence of molten chambers, Geol. Soc. Amer. Bull. 82, 2905-2920.

Mott, R. P. (1976). The relationship of microearthquake activity to structural geology for the region around Socorro, New Mexico, M. S. Independent Study, Geoscience Dept., New Mexico Inst. Mining and Tech.

Reilinger, R. and J. E. Oliver (1976). Modern uplift associated with a proposed magma body in the vicinity of Socorro, N. M., Geology, 4, 583-586.

Richter, C. F. (1958). Elementary Seismology, S. J. Freeman and Co., San Francisco, 768p.

Sanford, A. R. (1963). Seismic activity near Socorro, in New Mexico Geol. Soc. Guidebook, 14th. Field Conf., 146-151.

Sanford, A. R. (1968). Gravity survey in central Socorro County, New Mexico, Circ. 91, New Mexico State Bur. Mines Mineral Resources, 14 p.

Sanford, A. R., O. Alptekin, and T. R. Toppozada (1973). Use of reflection phases on microearthquake seismograms to map an unusual discontinuity beneath the Rio Grande rift, Bull. Seismol. Soc. Amer. 63, 2021-2034.

Sanford, A. R., A. J. Budding, J. P. Hoffman, O. S. Alptekin, C. A. Rush, and T. R. Toppazada (1972). Seismicity of the Rio Grande rift in New Mexico, Circ. 120, New Mexico State Bur. Mines Mineral Resources, 19 p.

Sanford, A. R. and C. R. Holmes (1962). Microearthquakes near Socorro, New Mexico, Jour. of Geophys. Res. 67, 4449-4459.

Sanford, A. R. and L. T. Long (1965). Microearthquake crustal reflections, Bull. Seismol. Soc. Amer. 55, 579-586.

Sanford, A. R., R. P. Mott, P. J. Shuleski, E. J. Rinehart, F. J. Caravella, R. M. Ward, and T. C. Wallace (1976). Geophysical evidence for a magma body in the crust in the vicinity of Socorro, New Mexico, Paper Presented at the ONR-CSM Symposium on "The Nature and Physical Properties of the Earth's Crust". Vail, Colorado, Aug. 2 - Aug. 6.

Shuleski, P. J. (1976). Seismic fault motion and SV wave screening by shallow magma bodies in the vicinity of Socorro, New Mexico, M. S. Independent Study, Geoscience Dept., New Mexico Inst. Mining and Tech.

Stuart, W. D., M. J. S. Johnston (1975). Intrusive origin of the Matsashiro earthquake swarm, Geology, Feb. 1975, 63-67.